Impacts of Coral Growth on Geochemistry: Lessons From the Galápagos Islands

Emma V. Reed[1] [ID] **, Diane M. Thompson[1]** [ID] **, Julia E. Cole[2]** [ID] **, Janice M. Lough[3,4]** [ID] **, Neal E. Cantin[3], Anson H. Cheung[5]** [ID] **, Alexander Tudhope[6], Lael Vetter[1]** [ID] **, Gloria Jimenez[7]** [ID] **, and R. Lawrence Edwards[8]**

[1]Department of Geosciences, University of Arizona, Tucson, AZ, USA, [2]Department of Earth and Environmental Sciences, University of Michigan, Ann Arbor, MI, USA, [3]Australian Institute of Marine Science, Townsville MC, Qld, Australia, [4]ARC Centre of Excellence for Coral Reef Studies, James Cook University, Townsville, Qld, Australia, [5]Department of Earth, Environmental, and Planetary Sciences, Brown University, Providence, RI, USA, [6]School of Geosciences, University of Edinburgh, Edinburgh, UK, [7]Chubb Limited, Philadelphia, PA, USA, [8]Department of Earth Sciences, University of Minnesota, Minneapolis, MN, USA

Abstract Coral geochemical climate reconstructions can extend our knowledge of global climate variability and trends over time scales longer than those of instrumental data. However, such reconstructions can be biased by coral growth and skeletal architecture, such as growth troughs, off-axis corallite orientation, and changing growth direction. This study quantifies the impact of skeletal architecture and growth on geochemistry using measurements of coral skeletal density, extension rate, and calcification rate, and uses these metrics to improve paleoclimate reconstructions. We present paired geochemistry-density records at Wolf Island, Galápagos, from three *Porites lobata* corals: two new paired density and geochemistry records from one fossil coral, and new density data from two previously published modern geochemistry records. We categorize each sampling transect used in this record by the quality of its orientation with respect to skeletal architecture. We observe relationships between geochemistry and density that are not detected using extension or calcification rate alone. These density-geochemistry relationships likely reflect both the response of coral growth to environmental conditions and the nonclimatic impact of skeletal architecture on geochemistry in suboptimal sampling transects. Correlations of density with Sr/Ca, Ba/Ca, and Mg/Ca are consistent with the Rayleigh fractionation model of trace element incorporation into coral skeletons. Removing transects with suboptimal skeletal architecture increases mean reconstructed SST closer to instrumental mean SST, and lowers errors of reconstruction by up to 20%. These results demonstrate the usefulness of coral density data for assessing skeletal architecture and growth when generating coral paleoclimate records.

1. Introduction

Coral Sr/Ca provides a well-established proxy for sea surface temperature (SST) (e.g., Beck et al., 1992; Corrège, 2006; Schrag, 1999), and is widely applied to reconstruct past climate in the Pacific (e.g., De-Long et al., 2012; Jimenez et al., 2018; Linsley et al., 2015) and across the global tropics (e.g., Emile-Geay et al., 2017; Loope et al., 2020; Tierney et al., 2015) (as reviewed by Felis (2020)). Coral-climate reconstructions provide insights into changes in interannual climate variability such as the El Niño-Southern Oscillation (ENSO) (e.g., Cobb et al., 2003, 2013; Grothe et al., 2020), Indian Ocean Dipole (e.g., Abram et al., 2003, 2007, 2020), decadal climate variability (e.g., DeLong et al., 2012; Felis et al., 2010; Linsley et al., 2015; Nurhati et al., 2011), and long-term climate trends (e.g., Carilli et al., 2014; Jimenez et al., 2018; Thompson et al., 2015; Wu, 2013) over time periods that predate the instrumental record. Other trace elemental ratios (hereafter "TE/Ca"), specifically Ba/Ca and Mg/Ca, are often measured alongside Sr/Ca. Coral Ba/Ca can record changes in seawater barium concentration associated with upwelling or coastal runoff (e.g., Alibert & Kinsley, 2008; Fleitmann et al., 2007; LaVigne et al., 2016; Maina et al., 2012; McCulloch et al., 2003; Montaggioni et al., 2006; Prouty et al., 2010; Shen et al., 1992), whereas Mg/Ca appears to reflect a combination of coral "vital effects" and possibly SST (e.g., Fallon et al., 2003; Marchitto et al., 2018; Mitsuguchi et al., 1996; Montagna et al., 2014).

Methodology: Julia E. Cole, Janice M. Lough, Neal E. Cantin, Lael Vetter
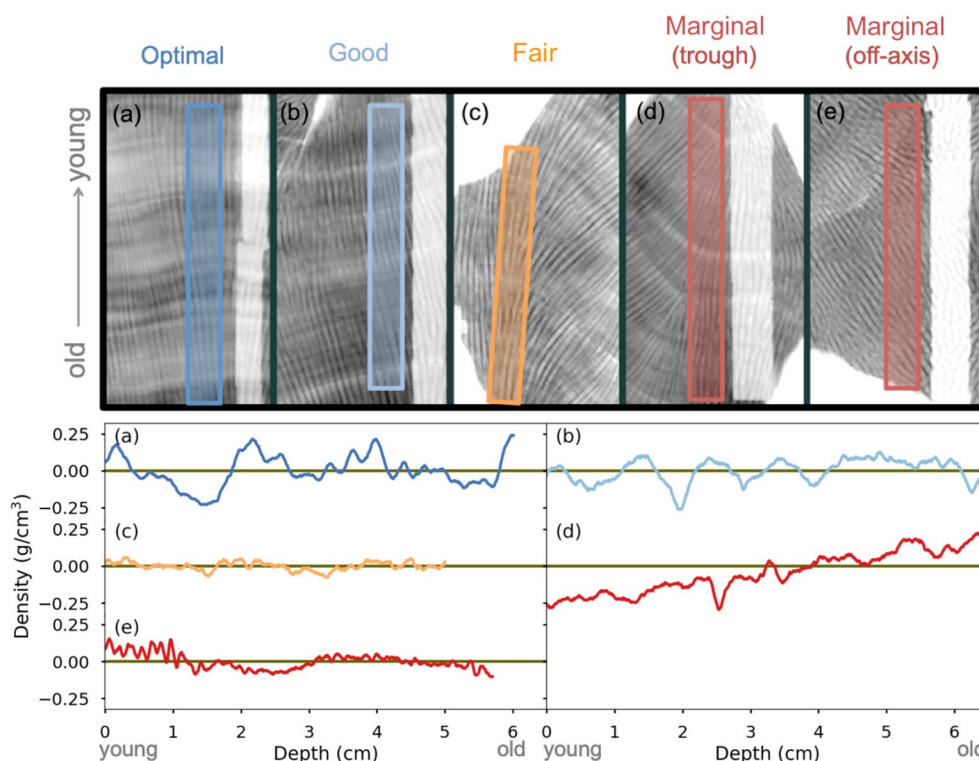**Writing – original draft:** Emma V. Reed, Diane M. Thompson
Writing – review & editing: Emma V. Reed, Diane M. Thompson, Julia E. Cole, Janice M. Lough, Neal E. Cantin, Anson H. Cheung, Alexander Tudhope, Lael Vetter, Gloria Jimenez, R. Lawrence Edwards

Figure 1. Examples of quality designations for density (colored) and geochemistry (pale transects parallel to density paths) transects. Top: Contrast-enhanced X-ray positives, with darker grays corresponding to denser skeleton. Bottom: density measurements, with the long-term mean subtracted, plotted by depth along each transect (i.e., prior to age modeling). Quality designations include: (a) optimal, with clear density bands and parallel corallites (from WLF10 BT1a); (b) good, with slight changes in growth direction, and a sampling path that is not colocated with the apex of a corallite fan (from WLF04 FT2b); (c) fair, with disorganized growth and weak density banding (from WLF04 BT4); and two examples of marginal transects, including a transect that approaches a low-density growth trough, (d) (from WLF04 BT1) and a transect with strongly angled corallites relative to the sampling plane (e) (from WLF05 AT2).

However, coral geochemical records can be affected by growth-related artifacts, such as coral growth rate. For example, portions of the geochemical record with extension rates below a critical threshold (for massive *Porites*, less than ~0.5–0.6 cm yr^{-1}) can display anomalously high Sr/Ca and δ^{18}O values (Felis et al., 2003; Goodkin et al., 2005; McConnaughey, 1989), biasing climate reconstructions toward cooler SST (e.g., Alibert & Kinsley, 2008; Alibert & McCulloch, 1997; Cohen & Hart, 2004; DeLong et al., 2013; de Villiers et al., 1995; Goodkin et al., 2005; Weber, 1973). In addition, thermal stress can impede coral growth and alter the incorporation of trace elements into coral skeletons, impacting TE/Ca proxies including Sr/Ca, Mg/Ca, and Ba/Ca (e.g., D'Olivo & McCulloch, 2017; D'Olivo et al., 2019; Ferrier-Pagès et al., 2018; Marshall & McCulloch, 2002). Another growth-related artifact is skeletal architecture, such as lobate growth, converging corallite fans ("growth troughs") (Figure 1d), changes in growth direction, and corallites angled relative to the sampling plane (Figure 1e). Many of these problematic features result from slabbing three-dimensional structures (e.g., corallite fans in lobate colonies) into two-dimensional slices, which is standard procedure for X-ray densitometry and geochemical sampling. Such features are sometimes avoidable when milling carbonate powder for geochemical analysis—for example, by sampling a replicate transect along a more optimal path, sampling the opposing face of the coral slice, or even reslabbing the coral along an alternate axis (DeLong et al., 2013). However, many corals exhibit complex growth patterns (e.g., changing growth direction over their lifetimes) that prevent recovery of a slice that faithfully tracks the axis of growth. Sampling in suboptimal regions can be unavoidable, and can bias the geochemical record and increase age uncertainties (e.g., Alibert & McCulloch, 1997; Allison & Finch, 2004; Comboul et al., 2014; DeLong et al., 2013; Kuffner et al., 2017). For example, increased Sr/Ca and Ba/Ca have been observed in growth troughs (Alibert &

Kinsley, 2008). Growth rate and skeletal architecture can therefore combine to influence geochemistry in complex ways, making it necessary to identify and account for these factors in coral geochemical records.

To screen for possible growth impacts, published reconstructions often include measurements of annual linear extension rate (the distance between successive annual tie points, such as Sr/Ca maxima or minima, or high/low density bands) (Allison & Finch, 2004; Dunbar et al., 1994; Goodkin et al., 2007; Grove et al., 2013). However, annual extension rate can fail to capture known growth-related artifacts (Alibert & McCulloch, 1997; Cohen & Hart, 1997). For example, corallite growth terminates where corallite fans converge, and these corallites become thin-walled, distorted, and less dense (Darke & Barnes, 1993). These growth troughs may exhibit anomalously high Sr/Ca values, despite neither compression nor expansion of annual density banding (Figure 1d)—and thus no change of extension rate—as a sampling path approaches a trough (Alibert & McCulloch, 1997; Cohen & Hart, 1997; DeLong et al., 2013). Extension rate also cannot accurately quantify growth when not measured along the apex of a corallite fan; instead, the angling of corallites relative to the sampling plane yields an apparent extension rate that can deviate from its actual value (DeLong et al., 2013). Furthermore, extension rate is not a holistic metric for coral growth rate. Rather, coral growth is defined by the calcification rate, given by $C = ED$, where C is the annual calcification rate (in g cm^{-2} yr^{-1}), E is the annual extension rate (cm yr^{-1}), and D is the mean skeletal density (g cm^{-3}) over the same time interval (Chalker et al., 1985; Lough, 2008; Lough & Barnes, 2000). On interannual time scales, extension rate generally varies more than annual mean density within and among *Porites* corals; for example, a study of 245 corals from the Great Barrier Reef found that extension rate varied by 26% of the average among corals, whereas density varied by only 13% (Lough & Barnes, 2000). As a result, interannual variability in calcification rate is primarily driven by extension rate.

Although the vast majority of studies focus on linear extension, coral skeletal density has long been used to quantify coral calcification rate (Lough & Cooper, 2011). These studies address questions ranging from changes in coral growth rate in a region through time (De'ath et al., 2009), to coral growth response to environmental stressors (Cantin & Lough, 2014; Carilli et al., 2017; Fabricius et al., 2011) and growth differences across sites (e.g., from fore-reef to back-reef) (Lough et al., 1999; Smith et al., 2007). Such studies harness the power of large sample sizes, relying on density records averaged among multiple transects from multiple corals in order to extract a common signal from density data, which varies across the three-dimensional structure within individual coral colonies and core samples.

This study uses an alternate approach by generating paired records of coral geochemistry and density along adjacent, parallel transects along the vertical growth axis of the coral. This approach allows for direct evaluation of growth-related artifacts in geochemical records, such as the impact of decreasing density as a sampling path approaches a growth trough, or of weak-to-absent annual density banding despite strong climate seasonality (e.g., where corallites are angled relative to the sampling plane, Figures 1c and 1e). The small sample size (one site with two partially replicated records) may make the interpretation of density data more sensitive to intertransect and intercoral differences, as well as coral ontogeny (i.e., age-related differences in density and extension rate). Therefore, the records presented here are not interpreted as local growth-rate reconstructions; rather, this approach is utilized to identify whether a geochemical record may be impacted by localized changes in coral skeletal architecture.

Here, we critically examine the potential impact of growth-related artifacts on geochemical reconstructions from the Galápagos Islands, Ecuador, using paired coral geochemical and density records. These records build upon a rich history of Galápagos coral reconstructions (e.g., Delaney et al., 1993; Druffel et al., 2004; Dunbar et al., 1994; Jimenez et al., 2018; Linn et al., 1990; McConnaughey, 1989; Shen et al., 1991; Wellington et al., 1996). However, no Galápagos coral records span the full 20th century (Cole & Tudhope, 2017); several records end during the 1982–1983 El Niño event (Dunbar et al., 1994; Shen et al., 1992) that caused wide-spread mortality across the archipelago (Glynn et al., 1988), limiting temporal overlap with satellite SST data. More recently, Jimenez et al. (2018) added a 70-year, partially replicated Sr/Ca record from modern Wolf Island corals, which identifies significant warming trends between 1940 and 2010.

The accuracy of such coral-climate reconstructions is paramount in the Galápagos Islands. Numerous studies point to the disproportionate importance of East Pacific sites for reconstructions of ENSO, Pacific decadal variability, and long-term global climate trends (e.g., Comboul et al., 2015; Loope et al., 2020).

Unfortunately, subannually resolved coral records are rare in this region (Tierney et al., 2015), as modern coral reefs are rare or locally extirpated (Glynn et al., 2018). Low and variable pH (Manzello, 2010; Manzello et al., 2008), high nutrients and abundance of macrofaunal boring organisms (DeCarlo et al., 2015), and high climate variability and thermal extremes (Glynn et al., 1988, 2018, for review) compound to create a suboptimal conditions for reef growth (hereafter "suboptimal environment"). This suboptimal reef environment, therefore, has limited diversity and structural complexity (Cortés, 1997; Darwin, 1889; Glynn, 2001; Glynn et al., 2017; Manzello et al., 2008), and coral colonies are more brittle and susceptible to erosion, both physical and biological. Therefore, the surviving massive corals in the Galápagos Islands display lobate and variable skeletal architecture, and often exhibit death horizons and macroborings (though such features can be present even in environments without such chronic stressors). Hereid et al. (2013) noted disagreements between instrumental data and coral-climate reconstructions from the eastern Pacific Ocean (Dunbar et al., 1994; Linsley et al., 1994, 2000), highlighting the importance of accounting for possible nonclimatic influences on coral geochemistry. The complex growth patterns of Galápagos corals, therefore, provide an opportunity to identify and remove coral growth-related artifacts that result from this suboptimal environment for coral growth, potentially improving geochemical climate reconstructions.

This study presents paired records of coral geochemistry (Sr/Ca, Ba/Ca, and Mg/Ca) and density from Wolf Island, Galápagos to quantify the impacts of growth-related artifacts on the fidelity of geochemical climate reconstructions. We present new density data from two colonies analyzed by Jimenez et al. (2018), and additionally provide a new 85-year (1691–1776 C.E., U/Th uncertainty = ±7 year) paired geochemical and density record from a fossil coral at the same site. Leveraging the suboptimal environment, stressors, and resulting growth variability observed at this site, we aim to answer three overarching questions:

1. Can we identify geochemical aberrations that are coincident with growth-related artifacts, such as skeletal architecture and growth rate?
2. How do density, extension, and calcification rate compare in their ability to identify significant relationships between geochemistry (Sr/Ca, Mg/Ca, and Ba/Ca) and growth?
3. What impact does the inclusion or exclusion of growth-related artifacts have on Sr/Ca-based SST reconstructions?

2. Climate Setting

As observed throughout the Galápagos Islands, Wolf Island (1.38°N, 91.82°W) experiences a two-season climate, governed by changes in ocean currents and trade winds (Figure S1). A warm/wet season occurs between January and May as the Intertropical Convergence Zone (ITCZ) approaches Galápagos, weakening trade winds and bringing warmer and fresher water from the Panama Bight (Kessler, 2006; Trueman & D'Ozouville, 2010; Wyrtki, 1966); the cool/dry season occurs between June and December, as the ITCZ shifts northward. With a northerly ITCZ, the trade winds and the nearby South Equatorial Current $(2 - 4°N)$ strengthen; the Equatorial Undercurrent, which shoals as it reaches the main Galápagos Islands, also upwells colder, nutrient-rich waters. As a remote northern island, Wolf is less sensitive to the Equatorial Undercurrent and associated upwelling than the main islands, but is more strongly cooled by the South Equatorial Current (Figure S1) (Kessler, 2006). Peak climatological warm and cool seasons therefore occur in March and August (Figure S2), with SST varying between 27.6 and 24.5 °C, respectively (Figure S1).

Galápagos climate is highly sensitive to changes in SST during ENSO events. During an El Niño event, trade winds weaken and the thermocline deepens as the upwelling of cold water decreases. SST anomalies during El Niño events are persistently ≥0.5 °C as a result. These anomalously high SSTs lengthen the hot season and increase rainfall as the ITCZ is displaced southward (Trueman & D'Ozouville, 2010). The opposite occurs during La Niña, with increased upwelling, decreased SST (anomalies ≤ −0.5 °C), and low rainfall (Trueman & D'Ozouville, 2010).

Long-term climate trends in this region are dependent on the length of the instrumental record, seasonality, and location. Observations of regional SST are sparse before 1950 (ICOADS 1°; Freeman et al., 2017), and in-situ records from the main islands within the upwelling region show no pronounced annual warming trends but increasing seasonality from 1964 to 2007 (Wolff, 2010). Published coral records from the main Galápagos Islands show annually resolved ENSO activity as far back as 1587, with relatively stable mean
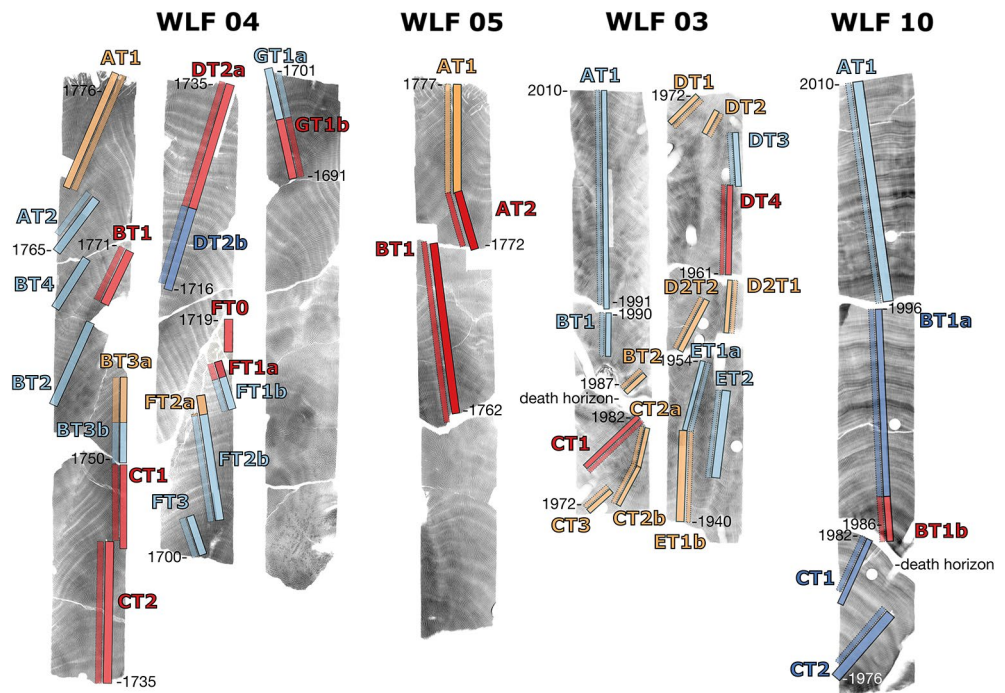
Figure 2. Contrast-enhanced X-ray positive images, with darker grays corresponding to denser skeleton, of fossil cores (WLF04 and WLF05) and modern cores (WLF03 and WLF10), with transects labeled. Colored outlines denote geochemical transects (wide paths with solid lines and opaque shading) and density transects (narrow paths with dotted lines and translucent shading). For WLF04 FT0, BT2, and BT4, geochemical and density transects are colocated. Colors denote quality: optimal transects are dark blue, good transects are light blue, fair transects are orange, and marginal transects are red. Years (C.E.) of the top and bottom of each core section are marked.

SST (<1 °C change) between 1880 and 1940 (Dunbar et al., 1994). In contrast, coral records from the northern archipelago show warming trends between 1940 and 2010 (Jimenez et al., 2018).

3. Methods

3.1. Coral Sampling

The fossil coral study site (WLF04 and WLF05; 1.386°N, 91.815°W) is located along the east side of Wolf Island at a water depth of 13 m. In May 2010, cores were obtained from a deceased *Porites lobata* colony ~2 m in height with little visible bioerosion. The coral had split vertically into two sections postmortality, and a complete core was taken from the top of each half along the vertical growth direction, with a core length of 174 cm for WLF04 and 163 cm for WLF05. Modern *Porites lobata* cores from the northeast side of the island (1.425°N, 92.067°W) were also collected from 10-m depth (WLF03) and 13 m (WLF10). Temperature reconstructions from these modern corals were published by Jimenez et al. (2018). All cores were assessed for diagenesis using scanning electron microscopy from sections adjacent to geochemical transects (as in Sayani et al. (2011)). Additional screening was performed in areas with extreme cold anomalies to ensure these departures reflected the primary climate signal (Figure S3).

3.2. Geochemistry

All coral cores were prepared, sampled, and analyzed for TE/Ca geochemistry using standard procedures (DeLong et al., 2013; Schrag, 1999). Cores were sliced ~5–10-mm thick, ultrasonicated in deionized water, and X-rayed to locate best available transects (Figure 2). Carbonate powder was sampled with a computerized micromill in continuous 1 mm increments along 8-mm-wide transects for WLF04 and WLF05, compared to either 4-mm-wide or 8-mm-wide transects for WLF03 and WLF10. WLF03 and WLF10 Sr/Ca have been previously published (Jimenez et al., 2018). The remaining records were measured at the University

of Arizona using a Jobin-Yvon Optima 2c inductively coupled plasma atomic emission spectrometer (ICP-AES) and a Thermo iCAP 7400 series ICP-AES, which replaced the Optima in 2016. We measured reference solutions during each instrument run to correct for analytical drift and matrix effects, and standardized each run to the mean of repeated measurements of an internal coral standard (Schrag, 1999). JCp-1, an interlaboratory reference coral standard, was also measured for all iCAP runs for comparison to the known value (Text S1). Analytical precisions, determined from the standard deviation (1σ) of repeated measurements of the internal coral standard, were ≤0.043 mmol/mol for Sr/Ca, ≤0.304 mmol/mol for Mg/Ca, and ≤0.188 μmol/mol for Ba/Ca; precisions for each core are given in Table S1. Further geochemical methods are given in Text S1. Notably, the WLF04 record was generated from both instruments, and we observed a mean offset between data replicated on both instruments (2 transects, 240 samples). We shifted WLF04 JY Sr/Ca and Mg/Ca data by this mean offset to match the mean of overlapping iCAP data (Text S1). After applying this correction, iCAP and JY data for WLF04 generally lie within 1σ analytical precision of each other (Figure S4). The top 3 cm of WLF04 was truncated from the record due to diagenesis in the uppermost portion of the record, likely due to adjacent borings (Figure 2). Finally, we screened all cores for geochemical outliers prior to age modeling (Text S1).

3.3. Density, Extension, and Calcification

Density measurements were not made along the same transects as geochemistry, as geochemical sampling was destructive and completed before density measurements; instead, we chose density transects parallel to their corresponding geochemical transects, with a 2-mm border separating them, on the side that most closely followed the central axis of the same corallite fan that was sampled for geochemistry (Figure 2). This approach, though unavoidable, may introduce some subannual age model uncertainties to the density record in cases where the density bands are not fully perpendicular to sampling path. To minimize the impacts of this chronological uncertainty, we present density results at annual rather than monthly resolution.

Densitometry was performed at the Australian Institute of Marine Science using standard procedures, including X-ray densitometry for all cores, and gamma densitometry for cores WLF04 and WLF05 for comparison to X-ray measurements. X-ray density was measured following an X-radiography method adapted from Anderson et al. (2017), and details are given in Text S2. In brief, grayscale values were extracted from background-corrected X-ray positives using the Fiji software package (Schindelin et al., 2012). Six standards of compressed *Porites* skeletal powder were used for calibration, applying a linear fit to known density × thickness for each standard vs. the natural log of each standard's mean grayscale value (Figure S5). Grayscale values were measured along 4-mm-wide transects at 0.005-cm intervals, converted to density using the grayscale calibration, and normalized by the thickness of the coral slice at each point along the transect. Density data near cracks or slice edges (both of which display low-density anomalies) were then removed. Uncertainty in X-ray density measurements was quantified using the 1σ uncertainty in the calibration slope and intercept (see Text S3). Gamma results for WLF04 and WLF05 were compared to those for X-ray density, and the mean, standard deviation, and correlation between methods were compared.

To calculate annual (summer-summer) extension, the distance between successive Sr/Ca minima (SST maxima) was measured, since we found that seasonality in Sr/Ca was more easily identifiable (i.e., regular and large seasonal amplitude) than in density data. Extension rate uncertainty calculations are described in Text S3. In brief, the SST maximum occurred between February and June in the instrumental data; thus, the 1σ chronological uncertainty of this warm season maximum (for Wolf Island, ±2.48 months) was used to compute uncertainties in extension rate. 1σ extension rate uncertainty ranged from −17% to 26%.

After age-modeling density using annual Sr/Ca tie points (Section 3.5), mean density was calculated over the same annual interval and multiplied by extension to yield annual calcification. Incomplete years (e.g., where density data are interrupted by a crack in the coral) were excluded from annual density, extension, and calcification calculations to avoid biasing the annual mean of density. Calcification rate uncertainties were conservatively estimated from density and extension rate uncertainties (see Text S3).

3.4. Transect Quality Assessment

We sorted transects by quality on a scale of 1 (optimal) to 4 (marginal), using key aspects of skeletal architecture described by DeLong et al. (2013). Transect quality was identified in X-ray images and confirmed by examining the slice surfaces with an optical microscope. In the few cases where the qualities of the density and geochemistry transects differed, the lowest common quality was used for both transects to yield a conservative quality estimate. Combined with the suboptimal environment for coral growth, these can therefore be considered as a worst-case scenario and conservative estimate of the impact of skeletal architecture on coral growth in these (and other) coral cores.

- Marginal: The transect approaches a trough where coral growth fans converge. Transects with corallites growing at a steep angle relative to the slicing plane (i.e., out of or into the slice) were also designated as "marginal." High-density stress bands adjacent to death horizons were similarly designated as "marginal"
- Fair: The transect meets two or more of the following criteria: it crosses an area where corallites are slightly angled relative to the slice; the transect is located slightly off the apex of a corallite fan; or the slice shows disorganized corallite growth (often visible as weaker-than-normal density banding)
- Good: The transect meets no more than one of the "fair" criteria, and corallite growth is parallel to the slice surface on the sampling side of the slice
- Optimal: The transect is located along the apex of corallite fans, growth bands are organized, and corallite growth is parallel to the slice surface on both sides of the slice

3.5. Age Modeling

Relative ages for all data were assigned by assuming that Sr/Ca minima correspond to March SST maxima (Figure S1), and linearly interpolating between these warm-season tie points. For WLF03 and WLF10, all tie points are identical to those published in Jimenez et al. (2018). All data were resampled at a temporal resolution of 12 samples per year. We use only one tie point per year due to the variable and poorly defined cool season minima, which can occur anytime between May and December (Figure S2). To assign absolute ages to the fossil record, we use a U/Th-dated sample from 622 mm below the youngest growth band for WLF04, and 46 mm from the top of slice E for WLF05 (following methods of Cheng et al. (2013) and Shen et al. (2002)). These depths were selected to obtain overlapping ages between the two cores, based on band counting from the top of each core and the estimated offset between the top ages of these cores.

3.6. Analyses

The relationship between Sr/Ca and growth metrics on annual time scales (density, extension, and calcification) was determined using ordinary least squares regression. We considered the use of weighted least squares (WLS) regression, which account for uncertainties in both dependent and independent variables (Thirumalai et al., 2011). However, WLS regression was not appropriate in this context because currently available methods require uncertainties to be symmetric (i.e., the upper and lower uncertainty bounds are equally distant from the actual value) (Thirumalai et al., 2011), but uncertainties in all three-growth metrics are strongly asymmetric. For this reason, we used ordinary least squares (OLS) regression to assess relationships between trace elements and growth metrics. We determined statistically significant relationships at the 95% confidence level. Effective degrees of freedom were adjusted to account for lag-1 autocorrelation (Bretherton et al., 1999; Dawdy & Matalas, 1964; World Meteorological Organization, 1966). Data were also binned by quality to determine whether particular transect qualities accounted for observed relationships.

To generate a final Sr/Ca record, transects were age-modeled individually to account for intertransect discrepancies in extension rate, then averaged between overlapping sections. This method was used to generate final records both for all data and for high-quality-only data. Modern corals were composited using the method described by Jimenez et al. (2018): each core was Z-scored, then averaged together over overlapping sections (1982–1975; 1987–2010); this average was converted to a composite Sr/Ca record by applying the average and standard deviation between both cores. This composite was generated for all data and again after removing low-quality transects. Since this study generated an age model for Sr/Ca before averaging between transects, our final age model includes some discontinuous data (e.g., a season at the end of a

transect), which may lead to small differences between results for Jimenez et al. (2018) and the results using all transect qualities for this study. This approach is needed in order to examine growth-geochemistry relationships in individual transects, as it avoids averaging overlapping transects of different qualities.

For modern corals, Sr/Ca was calibrated with SST at monthly resolution from the OISSTv2 AVHRR (Reynolds et al., 2007) using WLS regression for the period of continuous overlap between the two corals (May 1987 to March 2010); for WLS weights, we used the analytical precision of the Sr/Ca measurements (calculated across all runs for that coral) and monthly OISST uncertainties. We then recalculated these Sr/Ca-SST calibrations after removing low-quality transects to assess possible impacts of these transects on the calibration.

The Sr/Ca-SST calibration from high-quality transects was applied to all Sr/Ca records to generate reconstructed SST (SST_R) records. These SST_R records were compared to SST products, which were truncated to include only 1950–2010, when ICOADS sampling density in this region is at least monthly (i.e., >1 observation/month) (Freeman et al., 2017). Errors of reconstruction between SST_R and instrumental SST were assessed using root mean squared errors (RMSE). We then removed low-quality Sr/Ca transects from modern corals to create a high-quality transect record, and then applied the calibrations calculated using both the all-quality and high-quality Sr/Ca-SST data to this record. Finally, we compared the RMSEs of the resulting SST reconstructions with ERSSTv5 and HadISSTv1.1 (Huang et al., 2017; Rayner, 2003). Because the high-quality transect records are shorter than the all-quality records, we accounted for differences in sample size by generating 1,000 random subsets of the all-quality data with the same sample size as the high-quality transect data, and computed the mean and confidence intervals of the RMSEs for these random subsets. We compared the RMSEs for the random subset of all-quality transect data to those for the high-quality data.

4. Results

4.1. Geochemistry

The percentage of optimal or good sampling transects varied among cores. The WLF04 geochemical record is estimated to span 1691–1776 C.E., based on a U/Th date of 1732 ± 7 C.E. (Table S2) and band counting. About 48% of the WLF04 record (614 months, including overlaps between transects) is categorized as optimal or good (Figures 1–3 and Table S3). In contrast, the WLF05 record consists entirely of fair or marginal transects (Figures 2, S6, and Table S3). WLF05 was age modeled using a U/Th date of 1738 ± 5 C.E. (Table S2) and band counting. Because some portions of WLF05 are discontinuous, with off-axis corallite growth, WLF05 was cross-dated with WLF04 by aligning Sr/Ca records to yield a WLF05 top date of 1776 C.E. This absolute date was included for the sake of completeness, since our (within-core) analyses depend only on relative dating (i.e., band counting). For the modern corals, 48% of WLF03 transects (356 months) are optimal or good (Figures 2, S7, and Table S3), and 94% (343 months) of WLF10 are optimal or good (Figures 2, S8, and Table S3). The WLF03 record spans 1940–2010, with a growth hiatus between 1983 and 1987 (Figure S7). WLF10 spans 1976–2010, with a death horizon from 1982 to 1985 (Figure S8). Average annual extension rate for all corals ranged from 1.2 (WLF04) to 1.9 cm yr^{-1} (WLF10), such that geochemical sampling in 1 mm increments yielded approximately monthly sampling. Extension rate for all corals always exceeded 0.7 cm yr^{-1}.

4.2. Density, Extension, and Calcification

X-ray and gamma densities produced consistent results in individual cores. X-ray density standards generate strong calibration curves between density and grayscale on all X-ray images ($r^2 \geq 0.99$). X-ray density shows a significant mean offset from gamma density of 0.08–0.09 g cm^{-3} (paired sample t-test, $p < 0.01$) (Table S4). Aside from this offset, variance and standard deviations are nearly identical between the two methodologies (Table S4), and X-ray and gamma density are strongly correlated within each core (WLF04: $r = 0.91$, $p < 0.01$, $n = 1,066$; WLF05: $r = 0.92$, $p < 0.01$, $n = 179$). We observe some differences in the growth metrics among cores and transect qualities. Optimal and good transects generally show clear annual density bands; these bands become less distinct in fair transects or disappear altogether in off-axis transects (Figure 1). Furthermore, we see clear trends toward low density in transects that approach growth troughs (Figure 1d). Long-term mean density between coral cores differ by as much as 0.4 g cm^{-3}.
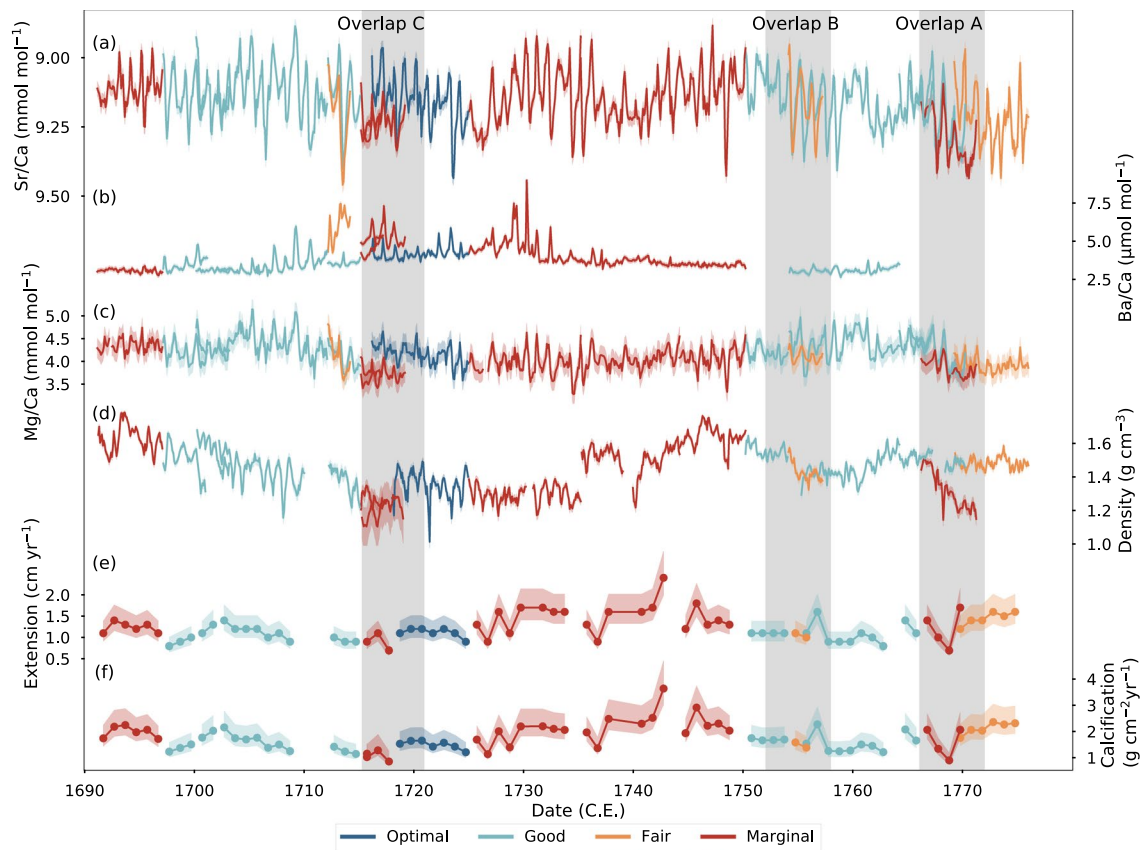
Figure 3. Age-modeled data for all WLF04 transects, including (a) Sr/Ca (*y* axis is inverted so warmer temperature is upward), (b) Ba/Ca, (c) Mg/Ca, (d) X-ray density, (e) annual extension rate, and (f) annual calcification rate. Colors denote the quality of each transect. Shading denotes 1σ uncertainty. Shaded bars denote three areas of overlap (Overlaps A–C) between transects of differing qualities, which are further analyzed in Figure 4. Similar plots for WLF03, 05, and 10 are given in the supporting information.

4.3. Influence of Growth-Related Artifacts on Geochemistry

Some portions of the WLF04 record include multiyear overlaps among transects of differing qualities, which we subset for further analysis (Figures 3 and 4). Six-year windows surrounding each overlap were chosen to ensure adequate sample sizes from each transect, though not all transects span the full time period of each overlap. Overlap A (1766–1772) includes a marginal-quality transect (Transect BT1) that approaches a growth trough in the youngest portion of this transect. As the transect approaches the trough, density and Mg/Ca decrease, and Ba/Ca and Sr/Ca increase (cooler apparent SST; Figures 1 and 3, note inverted Sr/Ca axis). Overlapping good (AT2, BT4) and fair (AT1) transects show higher median density, lower median Sr/Ca (higher inferred SST), and higher median Mg/Ca than this marginal transect. The same pattern holds true for Overlap C (1715–1721), in which two marginal transects (FT0 and FT1a) with strongly angled corallites relative to the sampling plane overlap or adjoin a high-quality transect (DT2b). Ba/Ca (only available for all overlapping transects in Overlap C) is higher in low-quality transects as well. Data from fair-quality transects do not appear to be compromised: Overlap B (1752–1758) includes one transect that transitions from fair (BT3a) to good (BT3b), and partially overlaps with a good transect (BT2). TE/Ca and density of the fair transect (BT3a) is not consistently different from overlapping/adjoining good transects (BT2 and BT3b). Overall, we observe low density, high Sr/Ca, high Ba/Ca, and low Mg/Ca anomalies in marginal transects (specifically growth troughs) relative to overlapping higher-quality transects.

Extending this test from overlapping sections to the full length of these records, however, reveals no systematic offsets among quality groups. We observe no consistent significant differences in density or TE/Ca between marginal or fair transects compared to higher-quality transects (Tables S5–S8). However, conflating factors likely affect these results, such as higher overall quality in the most recent portion of the record that
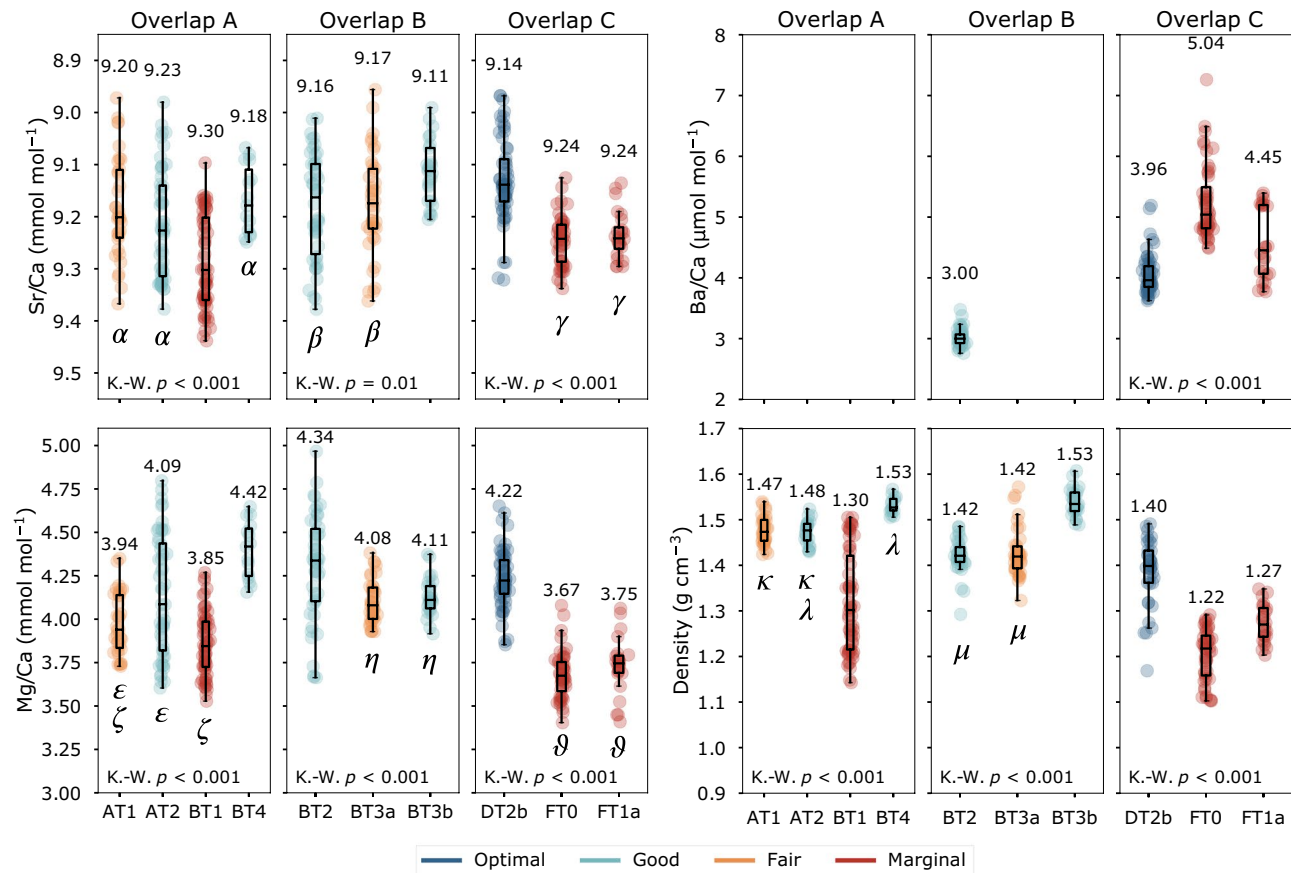
Figure 4. Comparison of Sr/Ca (top left, inverted so that warmer temperatures are upward), Mg/Ca (bottom left), Ba/Ca (top right), and density (bottom right) for three portions of the WLF04 record in which transects of differing qualities overlap: Overlap A (left column; 1766–1772), Overlap B (center column; 1752–1758), and Overlap C (right column; 1715–1721). Scatter point color denotes quality as in Figure 2, and each transect is annotated above its box plot with its median value. Significant differences in medians are tested using a Kruskal-Wallis test (where $p \leq 0.05$ indicates a statistically significant difference between medians), and the resulting p-values are given in the lower left corner of each plot. A Dunn's post-hoc test with a Bonferroni correction for multiple comparisons was then used to test for significant differences at $p \leq 0.05$. Greek symbols below each transect denote each group that the transect belongs to; e.g., in Sr/Ca results for Overlap A, AT1, AT2, and BT4 all belong to group α (i.e., are not significantly different from each other), whereas BT1 is significantly different from all other transects.

coincides with a warming trend (e.g., WLF03), as well as grouping together skeletal features with varying density and geochemical impacts (e.g., growth troughs and off-axis corallites). The approach in Figure 4 mitigates these complications.

We evaluate the impact of transect quality on the relationship between trace elements and growth by examining regressions between TE/Ca and growth metrics (density, extension, or calcification) for each coral (Figures 5, 6, S10, and S11). Annually resolved regressions between geochemistry and extension or calcification show inconsistent slopes and are not statistically significant, except in cases with small sample sizes (WLF05 Sr/Ca and MgCa, and WLF10 Ba/Ca) (Figure 5 and Table S9). In contrast, correlations between Sr/Ca and density show remarkably consistent slopes, ranging from −0.17 to −0.23 mmol mol^{-1} change in Sr/Ca per 1 g cm^{-3} increase in density. Mg/Ca and Ba/Ca relationships with density are also consistent among cores: all cores show positive regression slopes between Mg/Ca and density, and negative slopes between Ba/Ca and density (Table S9).

To increase sample sizes for all cores in subsequent analyses, we binned the data into "high quality" (optimal and good) and "low quality" (fair and marginal) for each coral record. We find that quality has no consistent effect on TE/Ca-growth regression slope or correlation strength or significance, regardless of the core, trace element, or growth metric (Figures 5, S10, S11 and Table S9). For example, excluding the low-quality transects yields marginally lower r-values when density and Sr/Ca are correlated (Figure 5 and Table S9), but
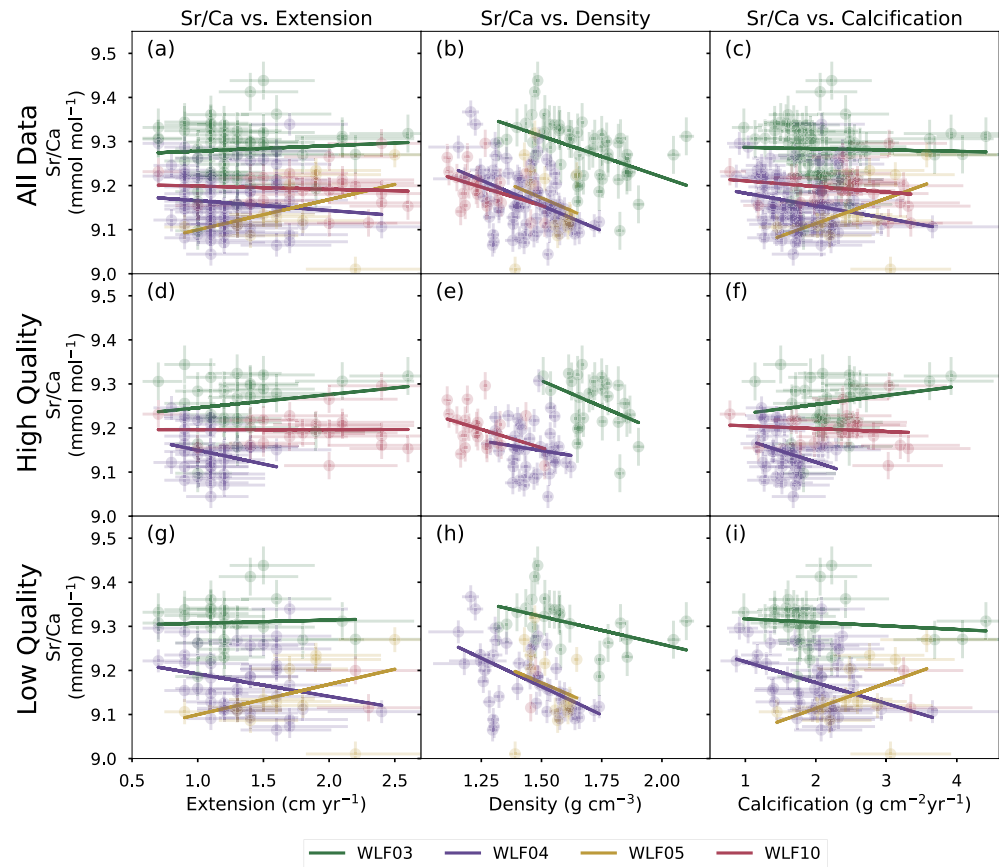
Figure 5. Ordinary Least Squares regressions of annual mean Sr/Ca with extension (left), annual mean density (center), and calcification (right) for all corals, including WLF03 (green), WLF04 (purple), WLF05 (yellow), and WLF10 (magenta). 1σ uncertainty is denoted by error bars. (a–c) All data, (d–f) high-quality transects (optimal and good) only, and (g–i) low-quality transects (fair and marginal) only. Sr/Ca is plotted with higher values (cooler temperature) upward. Regression statistics are given in Table S9.

the slopes of these regressions differ among cores, with some slopes becoming steeper (WLF03) and others becoming shallower (WLF04) with the removal of low-quality transects.

To examine the influence of transect quality on SST reconstructions, we first calculated modern Sr/Ca-SST calibrations with and without low-quality (fair and marginal) transects. The Sr/Ca-SST calibrations using all transects are largely consistent with calibrations based on high-quality transects only (Figure S9 and Table S10). We then applied these calibrations to reconstruct SST from Sr/Ca (SST_R), as in Jimenez et al. (2018), and compared to instrumental SST (ERSSTv5, 1950–2010). We find that the choice of transect quality used for calibration has no consistent impact on SST reconstruction: excluding low-quality transect data from Sr/Ca-SST calibrations does not consistently improve the agreement between reconstructed and instrumental SST (Table S11).

Nevertheless, we find that removing marginal and fair transects generally decreases root mean squared errors with SST data sets, bringing the reconstructed values closer to that observed in terms of both mean and variance. When the low-quality transects are removed from the WLF10 record (6% of the total), the RMSE changes little (Figure 7g). In contrast, removing low-quality transects from WLF03 (52% of the total record) consistently lowers the RMSE by up to 0.52 °C (Figure 7f). For the composite of WLF03 and WLF10, the RMSE with OISST decreases by 0.22 °C for both HadISST and ERSST. Removing low-quality transects decreases SST_R variability and range of the composite, and raises mean and median SST_R of both WLF03 and the WLF03-10 composite, bringing each closer to that of instrumental data (Figures 7a–7d).

5. Discussion

### 5.1. Relationship Between Density, Extension, and Calcification

Some previous studies have observed a weak inverse relationship between annual density and extension rate (Lough & Barnes, 1997; Scoffin et al., 1992). These studies reconstruct growth rate (integrated over many transects), rather than the combination of skeletal architecture and growth rate (as in this study), and thus may capture a seasonal trade-off between density and extension rate. However, such correlations are weak, likely due to the inherent imprecision of extension rate measurements (see next subsection). In contrast, our study finds no statistically significant relationship between annual density and extension rate in cores with large sample sizes (Figure 6d). The complex skeletal architecture of these Galápagos corals may mask or alter an inverse relationship between density and extension. For example, density and extension rate can decrease simultaneously in terminating corallite fans, and growth troughs can display anomalously low density without changes in extension rate (DeLong et al., 2013). Furthermore, extension rate (and thus calcification) estimates become less precise in transects where the direction of corallite growth is not parallel to the sampling plane, as we often observe in low-quality transects. As a result, we do not equate higher density with lower extension and calcification rates. Instead, changes in density observed here occur in the absence of predictable changes in measured extension and calcification rates.

5.2. Screening for Growth Impacts Using Extension, Density, and Calcification

Overlapping transects of differing qualities allow us to examine differences in geochemistry and density that may arise from skeletal architecture or growth variations. WLF04 transects that approach growth troughs, or transects in which corallite growth is perpendicular to the sampling plane, show significantly higher Sr/Ca than overlapping higher-quality transects (Figure 4). These offsets, +0.07–0.12 mmol mol^{-1}, equate to a cold bias of 1.1–2.2 °C, depending on the calibration applied. Because these transects are sampled from the same years' growth, these offsets do not reflect a climatological signal. Marginal-quality transects with growth troughs displayed significantly lower density compared to overlapping high-quality ones (Figure 4). Alongside close visual examination of corallite structure and X-ray images of sampling paths, density data can therefore aid in the identification of portions of the geochemical record that may be compromised by density-related artifacts. Future work could further subdivide transect qualities to address the influence of individual features of skeletal architecture (e.g., angled corallites, growth troughs, indistinct density banding) on geochemistry, as grouping disparate features together may mask significant differences among qualities (Tables S5–S8).

Relationships of trace elements with extension or calcification rate are neither consistent nor statistically robust, except in a few cases with small sample sizes. Statistically insignificant calcification correlations may arise because calcification rate is determined by extension rate. Extension rate measurements can be problematic for three reasons. First, annual extension rate may not be truly annual: the Sr/Ca minimum (SST maximum) that is used as a tie point to determine extension rate is not regularly timed. At Wolf Island, this problem is especially prevalent: though the peak warm season most frequently occurs in March, it falls anytime between February and June in the instrumental record (Figure S2). This chronological variability translates to a 1σ annual extension rate uncertainty of up to 26% (Text S3). Similar chronological errors can arise from calculating extension rate directly from density banding, especially because the seasonal timing of density banding can vary between sites (Tanzil et al., 2016) or even through time within individual corals (Reed et al., 2019). In contrast, the annual mean density error is no higher than 7%. This conservative error was estimated by applying the full range of possible tie points (February and June) to WLF04 density prior to age modeling, then calculating annual means and comparing to the annual means of the original WLF04 density record. Second, corallite growth that is angled relative to the sampling plane can change the "apparent" extension rate and introduce additional chronological errors (DeLong et al., 2013). Third, extension rate often does not change in architectural features with known geochemical artifacts, such as growth troughs, which are associated with changes in density (Figure 1d). For these reasons, extension rate, and therefore calcification rate, do not show the relationships between coral growth and geochemistry that are captured by density data.
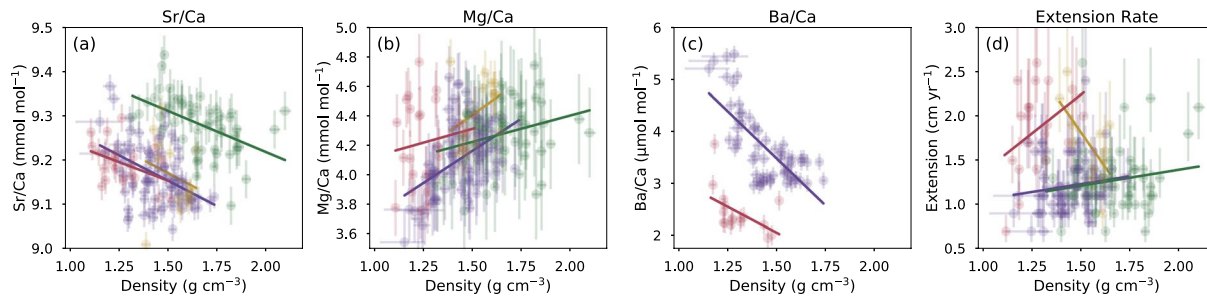
Figure 6. Ordinary Least Squares regressions of annual mean density with: (a) Sr/Ca, (b) Mg/Ca, (c) Ba/Ca, and (d) extension rate for WLF04 (purple), WLF03 (green), and WLF10 (magenta), and WLF05 (yellow) for all qualities of data. Error bars denote 1σ uncertainty. Sr/Ca is plotted with higher values (cooler temperature) upward.

When we regress density and Sr/Ca data from all transect qualities, we find consistently negative relationships, with higher density corresponding to lower Sr/Ca (higher inferred SST); similar negative relationships are found for Ba/Ca, whereas density-Mg/Ca regression slopes are positive. Other studies similarly demonstrate the impacts of coral growth on geochemistry. Previous work identified inverse relationships between Sr/Ca and coral extension rate (Goodkin et al., 2005) or calcification rate (Kuffner et al., 2012); other work demonstrates that high-density anomalies are often associated with coral stress (Cantin & Lough, 2014; Dodge et al., 1992; Hudson, 1981; Hudson et al., 1976). This stress can cause a breakdown of seasonality for Sr/Ca and other trace elements, including a warm bias during the cool season (D'Olivo & McCulloch, 2017). Finally, the negative relationship between density and Sr/Ca may also be partially due to decreasing density near growth troughs, as in DeLong et al. (2013) (Figure 1d), which raises Sr/Ca values and introduces a cold bias into the geochemical record. Similar growth trough anomalies have also been observed in Ba/Ca (Alibert & Kinsley, 2008). These growth troughs are especially prevalent in the WLF04 record (Figure 3), and the elimination of these growth troughs from the record may account for the weakened slope of the WLF04 Sr/Ca-density regression for high-quality transects (Figure 5e) compared to the all-quality and low-quality transects (Figures 5b and 5h).

Nonetheless, if relationships among trace elements and density resulted entirely from nonclimate, growth-related impacts on geochemistry, those correlations should be absent when low-quality transects are excluded (Figures 5d–5f). This is not the case. For example, high-quality transects still show negative relationships between density and Sr/Ca, though the correlation strength is marginally weaker than in the low-quality or all-quality transect data. Similarly, relationships remain consistent regardless of quality for both Mg/Ca and Ba/Ca. However, subdividing data by quality are subject to an important caveat: a relationship may require a certain sample size to be detectable. Power analysis reveals that sample sizes of the annually resolved data in Figure 5 consistently fall below the critical sample size ($n = 60$–100, depending on the r-value) needed for a power of 80%—i.e., a commonly accepted 20% probability of committing a Type II error (Cohen, 1977). Given the rarity of >100-year-long coral records with consistent quality throughout (especially in the eastern Pacific), this sample size limitation is unlikely to be easily resolved. Barring this sample size limitation, our results may indicate that relationships among trace elements and density reflect not only nonclimate, growth-related impacts on geochemistry, but also the impacts of climate on coral growth.

Modern corals, which overlap SST observations, allow us to test the alternate hypothesis that coral density changes with SST. We regressed density against SST for WLF03 and WLF10 during the full period of overlap (October 1981 to March 2010). Monthly data were included for comparison because the seasonal cycle provides a high-amplitude (∼3 °C) source of SST variability that could strongly influence coral density, but we find no relationship between SST and density on monthly time scales (Figure S12). Monthly scale relationships between density and other variables may be weakened by subannual chronological uncertainty introduced to the density age model by sampling geochemistry and density along separate transects. Nonetheless, both cores show a weak increase of density with SST on annual time scales, although the significance of these relationships is limited by the small sample size ($n \leq 18$) (Figure S12). This warm SST-high density relationship matches the direction of Sr/Ca-density relationships on annual (Figure 5) and monthly (Figure S13) time scales in modern corals, with low Sr/Ca (warmer inferred SST) corresponding
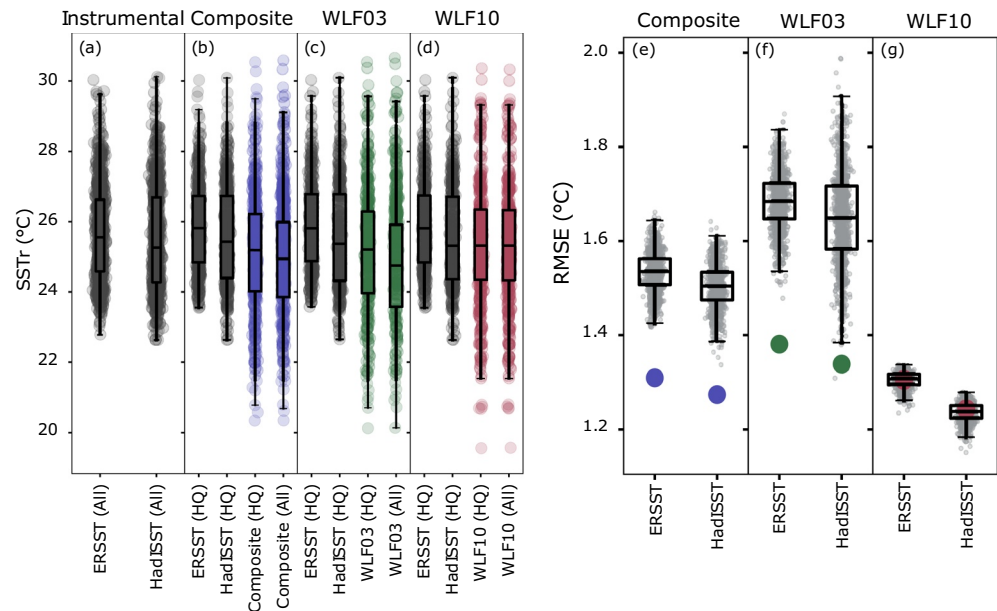
Figure 7. Box plot of instrumental data and reconstructed SST (SST$_R$) (a)–(d), and the root mean squared errors (RMSE) between reconstructed SST and instrumental SST (e)–(g). Left panel: (a) The instrumental SST for ERSST and HadISST (1950–2010). (b) SST$_R$ for the composite of the WLF03 and WLF10 coral records (colored), using either all data ("All") or high-quality transect data only ("HQ"). Included in each subfigure is each instrumental SST record (black), which is subset to match the dates included in the HQ record. Similar comparisons are also given for WLF03 (c) and WLF10 (d). Right panel: RMSE for reconstructed SST when compared to ERSST and HadISST, for: the composite of WLF03 and WLF10 (e) (blue), WLF03 (f) (green), and WLF10 (g) (red). For each SST data set, the RMSE of the data derived solely from high-quality transects is shown (colored points), and is compared to the distribution of RMSEs of 1,000 randomly generated subsets of the all-quality data sets with the same sample size as the high-quality data set (boxplots and gray scatter points). SST, sea surface temperature.

to high density. This directionality could result from high-density stress bands during warm events (Cantin & Lough, 2014; D'Olivo & McCulloch, 2017), or simply from higher density during warm seasons or years, as has been observed elsewhere (e.g., Buddemeier et al., 1974; Lough & Barnes, 1990; Reed et al., 2019). However, because the correlations between observed SST and density are weak, we cannot conclude that SST-driven density changes account for the Sr/Ca-density relationships seen here. Low-pH years associated with strong upwelling could drive this relationship; however, Galapagos coral growth metrics are generally insensitive to pH above 8.0, and regional seawater pH remains above this threshold (Humphreys et al., 2018; Manzello et al., 2014). Density variability within a given core could be driven by a combination of climate and skeletal architecture, but more work is needed to disentangle these components.

5.3. Possible Causes of Growth-Related Geochemical Artifacts

The use of multiple trace elements sheds light on possible explanations for observed element-density correlations. The directionality of these relationships is consistent with the partitioning of each trace element that occurs as new coral skeleton forms from the semiisolated calcifying fluid. The degree of partitioning is specific to each trace element: the inorganic aragonite-seawater exchange coefficient (K_D) for Mg/Ca is ~0.001, but greater than 1 for both Sr/Ca (~1.2) and Ba/Ca (~2.3) (Gaetani & Cohen, 2006). The aragonite skeleton that precipitates from this calcifying fluid is therefore enriched in Sr and Ba relative to seawater, but depleted in Mg, because Sr and Ba are preferentially partitioned into aragonite, whereas Mg is partitioned into the fluid (Cohen & Gaetani, 2010). Portions of the coral skeleton with low density, low Mg/Ca, high Sr/Ca, and high Ba/Ca likely reflect this process (Figure 6).

In contrast, this calcifying fluid can become more "isolated" from the surrounding seawater when the replenishment rate of the calcifying fluid is low relative to the rate of skeleton formation. In this Rayleigh-like process, deposition of the initial aragonite skeleton modifies the trace element composition of the calcifying

fluid, lowering fluid Sr and Ba and raising Mg concentrations. Subsequent skeleton is lower in Sr/Ca and Ba/Ca and higher in Mg/Ca as a result. These ratios are found in higher-density portions of the coral skeleton. Though comparisons and the statistical significance of *r*-values are limited by sample size, the signs of correlations for each trace element consistently match those predicted by this partitioning model, with negative Sr/Ca and Ba/Ca correlations and positive Mg/Ca correlations with density (Figure 6). Therefore, we interpret Figure 6 as showing the increasing impact of Rayleigh fractionation on trace element geochemistry as density increases. This process could explain the low density, high Sr/Ca, low Mg/Ca, and high Ba/Ca anomalies that occur in growth troughs compared to corallite fans (Figure 4): within a low-density growth trough, the rate of skeleton formation is low relative to the replenishment rate of the calcifying fluid (i.e., weaker Rayleigh fractionation).

These findings raise the question of whether faster or slower overall coral growth (i.e., calcification) corresponds to greater Rayleigh fractionation. Unfortunately, the link between density and overall coral growth in this study is unresolved. We might expect the observed relationship of low density with weaker Rayleigh fractionation to result from a higher refreshment rate of the calcifying fluid, such as by enhanced active transport by the Ca-ATPase pump. In addition to Ca^{2+}, this pump transports Sr^{2+}, with little discrimination between the two (with a transport stoichiometry Sr:Ca of 0.97) (Marchitto et al., 2018). Such active transport has been observed during periods of higher calcification rate in Great Barrier Reef corals (McCulloch et al., 2017). Because Great Barrier Reef corals often exhibit an inverse relationship between density and overall calcification (Lough, 2008; Lough & Barnes, 1997), we might expect greater active transport to cooccur at higher calcification rates and lower densities. Alternatively, low density could also correspond to low overall calcification rate for our Galápagos corals, during periods of low energy availability, low density, and slow growth, when the calcifying fluid is refreshed by passive transport at a rate that keeps pace with skeletal formation (resulting in weaker Rayleigh fractionation). Density and trace element anomalies present in growth troughs may support this interpretation. However, the lack of relationship between density and extension for the Galápagos corals (Figure 6d) means that we cannot infer which of these potential mechanisms is at play, and how density relates to overall calcification variability at this site. Nonetheless, these trace element-density relationships implicate Rayleigh fractionation as a contributor to the density-related geochemical artifacts observed here.

5.4. Effect of Growth Rate and Skeletal Architecture on SST Reconstructions

When reconstructing SST from modern Wolf corals (WLF03 and WLF10), we find only small differences among Sr/Ca-SST calibrations when all transects or only high-quality transects were utilized (Table S10). This consistency likely results from the high quality of both corals during the 1987–2010 calibration period; only 2 years of samples were excluded from WLF03, and 1 year from WLF10, when the calibrations from high-quality transects were calculated (Figures S7 and S8). When the new high-quality-transect calibrations were applied to high-quality transect data spanning the full length of both cores, errors of reconstruction with ERSST actually increase slightly (Table S11). This indicates that the choice of Sr/Ca-SST calibration cannot account for the decrease in errors of reconstruction between data from all-quality and high-quality transects observed in the composite and WLF03 data sets (Figures 7e–7g). This result is likely specific to these coral records and is not universally applicable: in instances where coral sampling paths are suboptimal during the calibration period, the calibration slope, intercept, and errors of reconstruction could be affected.

Instead, because data from low-quality transects are likely impacted by density-related artifacts, the inclusion of such data introduces nonclimate influences to the Sr/Ca record, increasing errors of reconstruction. These results demonstrate that more data does not always equate to better data; e.g., with WLF03, sample size decreases when low-quality transect data is excluded, but RMSE decreases. However, for WLF03, low-quality transects are more common earlier in the record, so we cannot discount the possibility that lower RMSE results not only from excluding low-quality transect data, but also from lower accuracy of the longer instrumental data sets (HadISST and ERSST) in this region prior to the satellite era (~1982). Therefore, the change in RMSE may partially result from eliminating inaccurate instrumental data in addition to eliminating low-quality coral transects. Nevertheless, we show that excluding low-quality transects from the WLF03-10 composite record does not alter the significant warming trends in the second half of the 20th century found by Jimenez et al. (2018) (Figures S14 and S15). In fact, the only major difference results from

the removal of a low-quality transect in the WLF03 record between ∼1955 and 1970, which hinders the detection of trends on time scales of 10 years or less (Figures S14 and S15).

6. Conclusions

The paired coral density-geochemistry records presented here exemplify the complexities and variability characteristic of growth in lobate, massive corals, which can complicate coral paleoclimate reconstructions. Portions of this record show geochemical offsets in contemporaneous data from high-quality and low-quality transects, and these offsets cooccur with changes in density. We find that extension rate (and therefore calcification rate, which is primarily driven by extension) is subject to numerous biases and consistently fails to capture the relationships with geochemistry that are observed using density. Density-geochemistry relationships may result from either nonclimate, density-related impacts on geochemistry, or from climate impacts on coral density, and further work is needed to disentangle these competing factors. Nonetheless, when transects with suspected density-related artifacts (after DeLong et al. (2013)) are excluded from climate reconstructions, errors of reconstruction decrease by up to 20%. Regressions of other trace element ratios (Mg/Ca and Ba/Ca) with density implicate Rayleigh fractionation as a possible driver of density-related geochemical artifacts. Our Galápagos study site ultimately provides an opportunity to study coral growth and geochemistry in suboptimal and increasingly stressful environments for coral growth. Further work is needed to assess the applicability of these results in other coral genera and other sites (especially sites with fewer extremes in climate and coral growth than the Galápagos region).

Our results emphasize the importance of assessing skeletal architecture when generating coral-based climate reconstructions. Because coral skeletons are fundamentally three-dimensional structures, it can be difficult to find an optimal sampling path along the apex of a corallite fan in a two-dimensional skeletal slice throughout the entire core. Computed tomography (CT) can circumvent this problem by quantifying density, extension, and calcification along complex, three-dimensional sampling paths. However, because skeletal powder for geochemistry is sampled along two-dimensional paths (i.e., after slicing the coral core), paired CT-geochemical studies remain an impractical prospect for avoiding growth-related artifacts without advances in geochemical sampling methods. Instead, two-dimensional geochemical sampling will likely be standard practice for the near future, and skeletal architecture along these sampling paths will need to be carefully addressed. This study demonstrates that densitometry can aid in the identification of growth-geochemistry relationships and nonclimatic artifacts, such as decreasing density and cold biases associated with converging corallite fans. Ideally, densitometry that precedes geochemical sampling would permit the measurement of skeletal density and geochemistry along identical transects; this approach would enable a better comparison of these growth-geochemistry relationships on subannual time scales. However, even in the absence of density data, being selective with the inclusion of suspected growth-impacted geochemical data can improve climate reconstructions. These results can assist in generating more accurate climate reconstructions from corals with complex skeletal architecture.

Conflict of Interest

The authors declare no conflicts of interest relevant to this study.

Data Availability Statement

All data developed in this study are publicly accessible (Reed et al., 2021) (Creative Commons Attribution 4.0 International License). Data will also be accessible via the National Center for Environmental Information paleoclimatology database (https://www.ncdc.noaa.gov/data-access/paleoclimatology-data/datasets).

References

Abram, N. J., Gagan, M., McCulloch, M., Chappell, J., & Hantoro, W. (2003). Coral reef death during the 1997 Indian Ocean dipole linked to Indonesian wildfires. *Science*, *301*(5635), 952–955. https://doi.org/10.1126/science.109198310.1126/science.1083841

Abram, N. J., Gagan, M. K., Liu, Z., Hantoro, W. S., McCulloch, M. T., & Suwargadi, B. W. (2007). Seasonal characteristics of the Indian Ocean Dipole during the Holocene epoch. *Nature*, *445*(7125), 299–302. https://doi.org/10.1038/nature05477

Abram, N. J., Wright, N. M., Ellis, B., Dixon, B. C., Wurtzel, J. B., England, M. H., et al. (2020). Coupling of Indo-Pacific climate variability over the last millennium. *Nature*, *579*(7799), 385–392. https://doi.org/10.1038/s41586-020-2084-4

Alibert, C., & Kinsley, L. (2008). A 170-year Sr/Ca and Ba/Ca coral record from the western Pacific warm pool: 1. What can we learn from an unusual coral record? *Journal of Geophysical Research*, *113*, C04008. https://doi.org/10.1029/2006JC003979

Alibert, C., & McCulloch, M. T. (1997). Strontium/calcium ratios in modern *Porites* corals From the Great Barrier Reef as a proxy for sea surface temperature: Calibration of the thermometer and monitoring of ENSO. *Paleoceanography*, *12*(3), 345–363. https://doi.org/10.1029/97PA00318

Allison, N., & Finch, A. A. (2004). High-resolution Sr/Ca records in modern *Porites lobata* corals: Effects of skeletal extension rate and architecture. *Geochemistry, Geophysics, Geosystems*, *5*, Q05001. https://doi.org/10.1029/2004GC000696

Anderson, K. D., Cantin, N. E., Heron, S. F., Pisapia, C., & Pratchett, M. S. (2017). Variation in growth rates of branching corals along Australia's Great Barrier Reef. *Scientific Reports*, *7*(1), 2920. https://doi.org/10.1038/s41598-017-03085-1

Beck, J. W., Edwards, R. L., Ito, E., Taylor, F. W., Recy, J., Rougerie, F., et al. (1992). Sea-surface temperature from coral skeletal strontium/calcium ratios. *Science*, *257*(5070), 644–647. https://doi.org/10.1126/science.257.5070.644

Bretherton, C. S., Widmann, M., Dymnikov, V. P., Wallace, J. M., & Bladé, I. (1999). The effective number of spatial degrees of freedom of a time-varying field. *Journal of Climate*, *12*(7), 1990–2009. https://doi.org/10.1175/1520-0442(1999)012<1990:TENOSD>2.0.co;2

Buddemeier, R. W., Maragos, J. E., & Knutson, D. W. (1974). Radiographic studies of reef coral exoskeletons: Rates and patterns of coral growth. *Journal of Experimental Marine Biology and Ecology*, *14*(2), 179–199. https://doi.org/10.1016/0022-0981(74)90024-0

Cantin, N. E., & Lough, J. M. (2014). Surviving coral bleaching events: *Porites* growth anomalies on the Great Barrier Reef. *PLoS One*, *9*(2), e88720. https://doi.org/10.1371/journal.pone.0088720

Carilli, J. E., Hartmann, A. C., Heron, S. F., Pandolfi, J. M., Cobb, K., Sayani, H., et al. (2017). *Porites* coral response to an oceanographic and human impact gradient in the Line Islands. *Limnology and Oceanography*, *62*, 2850. https://doi.org/10.1002/lno.10670

Carilli, J. E., McGregor, H. V., Gaudry, J. J., Donner, S. D., Gagan, M. K., Stevenson, S., et al. (2014). Equatorial Pacific coral geochemical records show recent weakening of the Walker Circulation. *Paleoceanography*, *29*, 1031–1045. https://doi.org/10.1002/2014PA002683

Chalker, B., Barnes, D., & Isdale, P. (1985). Calibration of x-ray densitometry for the measurement of coral skeletal density. *Coral Reefs*, *4*(2), 95–100. https://doi.org/10.1007/BF00300867

Cheng, H., Lawrence Edwards, R., Shen, C.-C., Polyak, V. J., Asmerom, Y., Woodhead, J., et al. (2013). Improvements in 230Th dating, 230Th and 234U half-life values, and U-Th isotopic measurements by multi-collector inductively coupled plasma mass spectrometry. *Earth and Planetary Science Letters*, *371–372*, 82–91. https://doi.org/10.1016/j.epsl.2013.04.006

Cobb, K. M., Charles, C. D., Cheng, H., & Edwards, R. L. (2003). El Niño/Southern Oscillation and tropical Pacific climate during the last millennium. *Nature*, *424*(6946), 271–276. https://doi.org/10.1038/nature01779

Cobb, K. M., Westphal, N., Sayani, H. R., Di Lorenzo, J. T. E., Cheng, H., Edwards, R. L., & Charles, C. D. (2013). Highly variable El Niño-Southern Oscillation throughout the holocene. *Science*, *339*(6115), 67–70. https://doi.org/10.1126/science.1228246

Cohen, A. L., & Gaetani, G. A. (2010). Ion partitioning and the geochemistry of coral skeletons: Solving the mystery of the vital effect. *EMU Notes in Mineralogy*, *11*, 377–397. https://doi.org/10.1180/EMU-notes.10.11

Cohen, A. L., & Hart, S. R. (1997). The effect of colony topography on climate signals in coral skeleton. *Geochimica et Cosmochimica Acta*, *61*(18), 3905–3912. https://doi.org/10.1016/S0016-7037(97)00200-7

Cohen, A. L., & Hart, S. R. (2004). Deglacial sea surface temperatures of the western tropical Pacific: A new look at old coral. *Paleoceanography*, *19*, PA4031. https://doi.org/10.1029/2004PA001084

Cohen, J. (1977). The t test for means. *Statistical power analysis for the behavioral sciences* (Chap. 2, pp. 19–74). Academic Press. https://doi.org/10.1016/B978-0-12-179060-8.50007-4

Cole, J., & Tudhope, A. W. (2017). Coral reefs of the Eastern Tropical Pacific. In P. W. Glynn (Ed.), *Coral reefs of the eastern tropical Pacific* (Chap. 19, pp. 535–548). Dordrecht, Netherlands: Springer Science+Business Media. https://doi.org/10.1007/978-94-017-7499-4

Comboul, M., Emile-Geay, J., Evans, M. N., Mirnateghi, N., Cobb, K. M., & Thompson, D. M. (2014). A probabilistic model of chronological errors in layer-counted climate proxies: Applications to annually banded coral archives. *Climate of the Past*, *10*(2), 825–841. https://doi.org/10.5194/cp-10-825-2014

Comboul, M., Emile-Geay, J., Hakim, G. J., & Evans, M. N. (2015). Paleoclimate sampling as a sensor placement problem. *Journal of Climate*, *28*(19), 7717–7740. https://doi.org/10.1175/JCLI-D-14-00802.1

Corrège, T. (2006). Sea surface temperature and salinity reconstruction from coral geochemical tracers. *Palaeogeography, Palaeoclimatology, Palaeoecology*, *232*, 408–428. https://doi.org/10.1016/j.palaeo.2005.10.014

Cortés, J. (1997). Biology and geology of eastern Pacific coral reefs. *Coral Reefs*, *16*, S39–S46. https://doi.org/10.1007/s003380050240

Darke, W. M., & Barnes, D. J. (1993). Growth trajectories of corallites and ages of polyps in massive colonies of reef-building corals of the genus *Porites*. *Marine Biology*, *117*, 321–326. https://doi.org/10.1007/BF00345677

Darwin, C., & Bonney, T. G. (1889). *The structure and distribution of coral reefs*. London: Smith Elder, & Co.

Dawdy, D. R., & Matalas, N. C. (1964). Statistical and probability analysis of hydrologic data, part III: Analysis of variance, covariance and time series. In V. T. Chow (Ed.), *Handbook of applied hydrology, a compendium of water-resources technology* (pp. 8.68–8.90). New York, NY: McGraw-Hill Book Company.

De'ath, G., Lough, J. M., & Fabricius, K. E. (2009). Declining coral calcification on the Great Barrier Reef. *Science*, *323*, 116–120.

DeCarlo, T. M., Gaetani, G. A., Holcomb, M., & Cohen, A. L. (2015). Experimental determination of factors controlling U/Ca of aragonite precipitated from seawater: Implications for interpreting coral skeleton. *Geochimica et Cosmochimica Acta*, *162*, 151–165. https://doi.org/10.1016/j.gca.2015.04.016

Delaney, M. L., Linn, L. J., & Druffel, E. R. M. (1993). Seasonal cycles of manganese and cadmium in coral from the Galapagos Islands. *Geochimica et Cosmochimica Acta*, *57*(2), 347–354. https://doi.org/10.1016/0016-7037(93)90436-Z

DeLong, K. L., Quinn, T. M., Taylor, F. W., Lin, K., & Shen, C.-C. (2012). Sea surface temperature variability in the southwest tropical Pacific since AD 1649. *Nature Climate Change*, *2*, 799–804. https://doi.org/10.1038/nclimate1583

DeLong, K. L., Quinn, T. M., Taylor, F. W., Shen, C.-C., & Lin, K. (2013). Improving coral-base paleoclimate reconstructions by replicating 350 years of coral Sr/Ca variations. *Palaeogeography, Palaeoclimatology, Palaeoecology*, *373*, 6–24. https://doi.org/10.1016/j.palaeo.2012.08.019

de Villiers, S., Nelson, B. K., & Chivas, A. R. (1995). Biological controls on coral Sr/Ca and δ18O reconstructions of sea surface temperatures. *Science*, *269*, 1247–1250. https://doi.org/10.1126/science.269.5228.1247

Dodge, R. E., Szmant, A., Garcia, R., Swart, P., Forester, A., & Leder, J. (1992). Skeletal structural basis of density banding in the Reef coral *Montastraea annularis*. In *Proceedings of the Seventh International Coral Reef Symposium, Guam* (Vol. 1, pp. 186–195).

D'Olivo, J. P., Georgiou, L., Falter, J., DeCarlo, T. M., Irigoien, X., Voolstra, C. R., et al. (2019). Long-term impacts of the 1997–1998 bleaching event on the growth and resilience of massive *Porites* corals from the central red sea. *Geochemistry, Geophysics, Geosystems*, *20*, 2936–2954. https://doi.org/10.1029/2019GC008312

D'Olivo, J. P., & McCulloch, M. T. (2017). Response of coral calcification and calcifying fluid composition to thermally induced bleaching stress. *Scientific Reports*, *7*(1), 2207. https://doi.org/10.1038/s41598-017-02306-x

Druffel, E. R. M., Griffin, S., Hwang, J., Komada, T., Beaupre, S. R., Druffel-Rodriguez, K. C., & Southon, G. M. J. (2004). Variability of monthly radiocarbon during the 1760S in corals from the Galapagos Islands. *Radiocarbon*, *46*(2), 627–631. https://doi.org/10.1017/s0033822200035670

Dunbar, R. B., Wellington, G. M., Colgan, M. W., & Glynn, P. W. (1994). Eastern Pacific sea surface temperature since 1600 A.D.: The δ18O record of climate variability in Galápagos Corals. *Paleoceanography*, *9*(2), 291–315. https://doi.org/10.1029/93PA03501

Emile-Geay, J., McKay, N., Kaufman, D., Von Gunten, L., Wang, J., Anchukaitis, K., et al. (2017). A global multiproxy database for temperature reconstructions of the Common Era. *Scientific Data*, *4*, 170088. https://doi.org/10.1038/sdata.2017.88

Fabricius, K. E., Langdon, C., Uthicke, S., Humphrey, C., Noonan, S., De'ath, G., et al. (2011). Losers and winners in coral reefs acclimatized to elevated carbon dioxide concentrations. *Nature Climate Change*, *1*, 165–169. https://doi.org/10.1038/NCLIMATE1122

Fallon, S. J., McCulloch, M. T., & Alibert, C. (2003). Examining water temperature proxies in *Porites* corals from the Great Barrier Reef: A cross-shelf comparison. *Coral Reefs*, *22*(4), 389–404. https://doi.org/10.1007/s00338-003-0322-5

Felis, T. (2020). Extending the instrumental record of ocean-atmosphere variability into the last interglacial using tropical corals. *Oceanography*, *33*(2), 68–79. https://doi.org/10.5670/oceanog.2020.209

Felis, T., Pätzold, J., & Loya, Y. (2003). Mean oxygen-isotope signatures in *Porites* spp. corals: Inter-colony variability and correction for extension-rate effects. *Coral Reefs*, *22*(4), 328–336. https://doi.org/10.1007/s00338-003-0324-3

Felis, T., Suzuki, A., Kuhnert, H., Rimbu, N., & Kawahata, H. (2010). Pacific Decadal Oscillation documented in a coral record of North Pacific winter temperature since 1873. *Geophysical Research Letters*, *37*, L14605. https://doi.org/10.1029/2010GL043572

Ferrier-Pagès, C., Sauzéat, L., & Balter, V. (2018). Coral bleaching is linked to the capacity of the animal host to supply essential metals to the symbionts. *Global Change Biology*, *24*(7), 3145–3157. https://doi.org/10.1111/gcb.14141

Fleitmann, D., Dunbar, R. B., McCulloch, M., Mudelsee, M., Vuille, M., McClanahan, T. R., et al. (2007). East African soil erosion recorded in a 300 year old coral colony from Kenya. *Geophysical Research Letters*, *34*, L04401. https://doi.org/10.1029/2006GL028525

Freeman, E., Woodruff, S. D., Worley, S. J., Lubker, S. J., Kent, E. C., Angel, W. E., et al. (2017). ICOADS release 3.0: A major update to the historical marine climate record. *International Journal of Climatology*, *37*(5), 2211–2232. https://doi.org/10.1002/joc.4775

Gaetani, G. A., & Cohen, A. L. (2006). Element partitioning during precipitation of aragonite from seawater: A framework for understanding paleoproxies. *Geochimica et Cosmochimica Acta*, *70*(18), 4617–4634. https://doi.org/10.1016/j.gca.2006.07.008

Glynn, P. W. (2001). Eastern Pacific coral reef ecosystems. In U. Seeliger, & B. Kjerfve (Eds.), *Coastal marine ecosystems of Latin America* (pp. 281–305). Berlin, Germany: Springer.

Glynn, P. W., Alvarado, J. J., Banks, S., Cortés, J., Feingold, J. S., Jiménez, C., et al. (2017). Eastern Pacific coral reef provinces, coral community structure and composition: An overview. In P. Glynn, D. Manzello, & I. Enochs (Eds.), Coral reefs of the eastern tropical Pacific. Coral reefs of the world (Vol. 8, pp. 107–176). Dordrecht, Netherlands: Springer.

Glynn, P. W., Cortés, J., Guzmán, H. M., & Richmond, R. H. (1988). El Niño (1982-83) associated coral mortality and relationship to sea surface temperature deviations in the tropical eastern Pacific. In *Proceedings 6th International Coral Reef Symposium* (Vol. 3, pp. 237–243).

Glynn, P. W., Feingold, J. S., Baker, A., Banks, S., Baums, I. B., Cole, J., et al. (2018). State of corals and coral reefs of the Galápagos Islands (Ecuador): Past, present and future. *Marine Pollution Bulletin*, *133*, 717–733. https://doi.org/10.1016/j.marpolbul.2018.06.002

Goodkin, N. F., Hughen, K. A., & Cohen, A. L. (2007). A multicoral calibration method to approximate a universal equation relating Sr/Ca and growth rate to sea surface temperature. *Paleoceanography*, *22*, PA1214. https://doi.org/10.1029/2006PA001312

Goodkin, N. F., Hughen, K. A., Cohen, A. L., & Smith, S. R. (2005). Record of little ice age sea surface temperatures at Bermuda using a growth-dependent calibration of coral Sr/Ca. *Paleoceanography*, *20*, PA4016. https://doi.org/10.1029/2005PA001140

Grothe, P. R., Cobb, K. M., Liguori, G., Di Lorenzo, E., Capotondi, A., Lu, Y., et al. (2020). Enhanced El Niño-Southern Oscillation variability in recent decades. *Geophysical Research Letters*, *47*, e2019GL083906. https://doi.org/10.1029/2019GL083906

Grove, C. A., Kasper, S., Zinke, J., Pfeiffer, M., Garbe-Schönberg, D., & Brummer, G.-J. A. (2013). Confounding effects of coral growth and high SST variability on skeletal Sr/Ca: Implications for coral paleothermometry. *Geochemistry, Geophysics, Geosystems*, *14*, 1277–1293. https://doi.org/10.1002/ggge.20095

Hereid, K. A., Quinn, T. M., & Okumura, Y. M. (2013). Assessing spatial variability in El Niño-Southern Oscillation event detection skill using coral geochemistry. *Paleoceanography*, *28*, 14–23. https://doi.org/10.1029/2012PA002352

Huang, B., Thorne, P. W., Banzon, V. F., Boyer, T., Chepurin, G., Lawrimore, J. H., et al. (2017). Extended Reconstructed Sea Surface Temperature, version 5 (ERSSTv5): Upgrades, validations, and intercomparisons. *Journal of Climate*, *30*, 8179–8205. https://doi.org/10.1175/jcli-d-16-0836.1

Hudson, J. H. (1981). Growth rates in *Montastraea annularis*: A record of environmental change in Key Largo Coral Reef marine Sanctuary, Florida. *Deep Sea Research Part B. Oceanographic Literature Review*, *28*(12), 882. https://doi.org/10.1016/0198-0254(81)91549-1

Hudson, J. H., Shinn, E. A., Halley, R. B., & Lidz, B. (1976). Sclerochronology: A tool for interpreting past environments. *Geology*, *4*(6), 361–364. https://doi.org/10.1130/0091-7613(1976)4<361:SATFIP>2.0.CO;2;10.1130/0091-7613(1976)4<361:satfip>2.0.co;2

Humphreys, A. F., Halfar, J., Ingle, J. C., Manzello, D., Reymond, C. E., Westphal, H., & Riegl, B. (2018). Effect of seawater temperature, pH, and nutrients on the distribution and character of low abundance shallow water benthic foraminifera in the Galapagos. *PLoS One*, *13*(9), e0202746. https://doi.org/10.1371/journal.pone.0202746

Jimenez, G., Cole, J. E., Thompson, D. M., & Tudhope, A. W. (2018). Northern Galápagos corals reveal twentieth century warming in the eastern tropical pacific. *Geophysical Research Letters*, *45*, 1981–1988. https://doi.org/10.1002/2017GL075323

Kessler, W. S. (2006). The circulation of the eastern tropical Pacific: A review. *Progress in Oceanography*, *69*(2–4), 181–217. https://doi.org/10.1016/j.pocean.2006.03.009

Kuffner, I. B., Bartels, E., Stathakopoulos, A., Enochs, I. C., Kolodziej, G., Toth, L. T., & Manzello, D. P. (2017). Plasticity in skeletal characteristics of nursery-raised staghorn coral, *Acropora cervicornis*. *Coral Reefs*, *36*(3), 679–684. https://doi.org/10.1007/s00338-017-1560-2

Kuffner, I. B., Jokiel, P. L., Rodgers, K. S., Andersson, A. J., & MacKenzie, F. T. (2012). An apparent "vital effect" of calcification rate on the Sr/Ca temperature proxy in the reef coral Montipora capitata. *Geochemistry, Geophysics, Geosystems*, *13*, Q08004. https://doi.org/10.1029/2012GC004128

LaVigne, M., Grottoli, A. G., Palardi, J. E., & Sherrell, R. M. (2016). Multi-colony calibrations of coral Ba/Ca with a contemporaneous in situ seawater barium record. *Geochimica et Cosmochimica Acta*, *179*, 203–216.

Linn, L. J., Delaney, M. L., & Druffel, E. R. M. (1990). Trace metals in contemporary and seventeenth-century Galápagos coral: Records of seasonal and annual variations. *Geochimica et Cosmochimica Acta*, *54*, 387–394.

Linsley, B. K., Dunbar, R. B., Wellington, G. M., & Mucciarone, D. A. (1994). A coral-based reconstruction of Intertropical Convergence Zone variability over Central America since 1707. *Journal of Geophysical Research*, *99*(C5), 9977–9994. https://doi.org/10.1029/94JC00360

Linsley, B. K., Ren, L., & Howe, S. S. (2000). El Nino Southern Oscillation (ENSO) and decadal-scale climate variability at 10N in the eastern Pacific from 1893 to 1994: A coral-based reconstruction from Clipperton Atoll. *Paleoceanography*, *15*(3), 322–335. https://doi.org/10.1029/1999PA000428

Linsley, B. K., Wu, H. C., Dassié, E. P., & Schrag, D. P. (2015). Decadal changes in South Pacific sea surface temperatures and the relationship to the Pacific decadal oscillation and upper ocean heat content. *Geophysical Research Letters*, *42*, 2358–2366. https://doi.org/10.1002/2015GL063045

Loope, G., Thompson, D., Cole, J., & Overpeck, J. (2020). Is there a low-frequency bias in multiproxy reconstructions of tropical Pacific SST variability? *Quaternary Science Reviews*, *246*, 2358–2366. https://doi.org/10.1016/j.quascirev.2020.106530

Lough, J. M. (2008). Coral calcification from skeletal records revisited. *Marine Ecology Progress Series*, *373*, 257–264. https://doi.org/10.3354/meps07398

Lough, J. M., & Barnes, D. J. (1990). Intra-annual timing of density band formation of *Porites* coral from the central Great Barrier Reef. *Journal of Experimental Marine Biology and Ecology*, *135*, 35–57.

Lough, J. M., & Barnes, D. J. (1997). Several centuries of variation in skeletal extension, density and calcification in massive *Porites* colonies from the Great Barrier Reef: A proxy for seawater temperature and a background of variability against which to identify unnatural change. *Journal of Experimental Marine Biology and Ecology*, *211*, 29–67.

Lough, J. M., & Barnes, D. J. (2000). Environmental controls on growth of the massive coral *Porites*. *Journal of Experimental Marine Biology and Ecology*, *245*, 225–243.

Lough, J. M., Barnes, D. J., Devereux, M. J., Tobin, B. J., & Tobin, S. (1999). Variability in growth characteristics of massive *Porites* on the Great Barrier Reef. *Tech. Rep. 28*. Townsville: CRC Reef Research Centre.

Lough, J. M., & Cooper, T. F. (2011). New insights from coral growth band studies in an era of rapid environmental change. *Earth-Science Reviews*, *108*, 170–184. https://doi.org/10.1016/j.earscirev.2011.07.001

Maina, J., de Moel, H., Vermaat, J. E., Bruggemann, J. H., Guillaume, M. M. M., Grove, C. A., et al. (2012). Linking coral river runoff proxies with climate variability, hydrology and land-use in Madagascar catchments. *Marine Pollution Bulletin*, *64*(10), 2047–2059. https://doi.org/10.1016/j.marpolbul.2012.06.027

Manzello, D. P. (2010). Ocean acidification hotspots: Spatiotemporal dynamics of the seawater CO_2 system of eastern Pacific coral reefs. *Limnology and Oceanography*, *55*, 239–248.

Manzello, D. P., Enochs, I. C., Bruckner, A., Renaud, P. G., Kolodziej, G., Budd, D. A., et al. (2014). Galápagos coral reef persistence after ENSO warming across an acidification gradient. *Geophysical Research Letters*, *41*, 9001–9008. https://doi.org/10.1002/2014GL062501

Manzello, D. P., Kleypas, J. A., Budd, D. A., Eakin, C. M., Glynn, P. W., & Langdon, C. (2008). Poorly cemented coral reefs of the eastern tropical Pacific: Possible insights into reef development in a high-CO_2 world. *Proceedings of the National Academy of Sciences of the United States of America*, *105*, 10450–10455.

Marchitto, T. M., Bryan, S. P., Doss, W., McCulloch, M. T., & Montagna, P. (2018). A simple biomineralization model to explain Li, Mg, and Sr incorporation into aragonitic foraminifera and corals. *Earth and Planetary Science Letters*, *481*, 20–29. https://doi.org/10.1016/j.epsl.2017.10.022

Marshall, J. F., & McCulloch, M. T. (2002). An assessment of the Sr/Ca ratio in shallow water hermatypic corals as a proxy for sea surface temperature. *Geochimica et Cosmochimica Acta*, *66*(18), 3263–3280. https://doi.org/10.1016/S0016-7037(02)00926-2

McConnaughey, T. (1989). 13C and 18O isotopic disequilibrium in biological carbonates: I. Patterns. *Geochimica et Cosmochimica Acta*, *53*(1), 151–162. https://doi.org/10.1016/0016-7037(89)90282-2

McCulloch, M. T., D'Olivo, J. P., Falter, J., Holcomb, M., & Trotter, J. A. (2017). Coral calcification in a changing World and the interactive dynamics of pH and DIC upregulation. *Nature Communications*, *8*, 15686. https://doi.org/10.1038/ncomms15686

McCulloch, M. T., Fallon, S., Wyndham, T., Hendy, E., Lough, J., & Barnes, D. (2003). Coral record of increased sediment flux to the inner Great Barrier Reef since European settlement. *Nature*, *421*, 727–730. https://doi.org/10.1038/nature01361

Mitsuguchi, T. E., Matsumoto, Abe, O., Uchida, T., & Isdale, P. J. (1996). Mg/Ca thermometry in coral skeletons. *Science*, *274*(5289), 961–963. https://doi.org/10.1126/science.274.5289.961

Montaggioni, L. F., Le Cornec, F., Corrège, T., & Cabioch, G. (2006). Coral barium/calcium record of mid-Holocene upwelling activity in New Caledonia, South-West Pacific. *Palaeogeography, Palaeoclimatology, Palaeoecology*, *237*, 436–455. https://doi.org/10.1016/j.palaeo.2005.12.018

Montagna, P., McCulloch, M., Douville, E., López Correa, M., Trotter, J., Rodolfo-Metalpa, R., et al. (2014). Li/Mg systematics in scleractinian corals: Calibration of the thermometer. *Geochimica et Cosmochimica Acta*, *132*, 288–310. https://doi.org/10.1016/j.gca.2014.02.005

Nurhati, I. S., Cobb, K. M., & Di Lorenzo, E. (2011). Decadal-scale SST and salinity variations in the central tropical Pacific: Signatures of natural and anthropogenic climate change. *Journal of Climate*, *24*(13), 3294–3308.

Prouty, N. G., Field, M. E., Stock, J. D., Jupiter, S. D., & McCulloch, M. (2010). Coral Ba/Ca records of sediment input to the fringing reef of the southshore of Moloka'i, Hawai'i over the last several decades. *Marine Pollution Bulletin*, *60*(10), 1822–1835. https://doi.org/10.1016/j.marpolbul.2010.05.024

Rayner, N. A. (2003). Global analyses of sea surface temperature, sea ice, and night marine air temperature since the late nineteenth century. *Journal of Geophysical Research*, *108*(D14), 4407. https://doi.org/10.1029/2002JD002670

Reed, E. V., Cole, J. E., Lough, J. M., & Cantin, N. E. (2019). Linking climate variability and growth in coral skeletal records from the Great Barrier Reef. *Coral Reefs*, *38*(1), 29–43.

Reed, E. V., Thompson, D. M., Cole, J. E., Lough, J. M., Cantin, N. E., Cheung, A. H., et al. (2021). Impact of coral growth on geochemistry: Lessons from the Galapagos Islands [Data set]. *Zenodo*. https://doi.org/10.5281/zenodo.4555511

Reynolds, R., Smith, T., Liu, C., Chelton, D., Casey, K., & Schlax, M. (2007). Daily high-resolution-blended analyses for sea surface temperature. *Journal of Climate*, *20*, 5473–5496. https://doi.org/10.1175/2007JCLI1824.1

Sayani, H. R., Cobb, K. M., Cohen, A. L., Elliott, W. C., Nurhati, I. S., Dunbar, R. B., et al. (2011). Effects of diagenesis on paleoclimate reconstructions from modern and young fossil corals. *Geochimica et Cosmochimica Acta*, *75*(21), 6361–6373. https://doi.org/10.1016/j.gca.2011.08.026

Schindelin, J., Arganda-Carreras, I., Frise, E., Kaynig, V., Longair, M., Pietzsch, T., et al. (2012). Fiji: An open-source platform for biological-image analysis. *Nature Methods*, *9*(7), 676–682. https://doi.org/10.1038/nmeth.2019

Schrag, D. P. (1999). Rapid analysis of high-precision Sr/Ca ratios in corals and other marine carbonates. *Paleoceanography*, *14*(2), 97–102. https://doi.org/10.1029/1998PA900025

Scoffin, T. P., Tudhope, A. W., Brown, B. E., Chansang, H., & Cheeney, R. F. (1992). Patterns and possible environmental controls of skeletogenesis of *Porites lutea*, South Thailand. *Coral Reefs*, *11*, 1–11. https://doi.org/10.1007/BF00291929

Shen, C. C., Lawrence Edwards, R., Cheng, H., Dorale, J. A., Thomas, R. B., Bradley Moran, S., et al. (2002). Uranium and thorium isotopic and concentration measurements by magnetic sector inductively coupled plasma mass spectrometry. *Chemical Geology*, *185*(3–4), 165–178. https://doi.org/10.1016/S0009-2541(01)00404-1

Shen, G., Cole, J., Lea, D., Linn, L., Mcconnaughey, T., & Fairbanks, R. (1992). Surface ocean variability at Galápagos from 1936-1982: Calibration of geochemical tracers in corals. *Paleoceanography*, *7*(5), 563–588.

Shen, G. T., Campbell, T. M., Dunbar, R. B., Wellington, G. M., Colgan, M. W., & Glynn, P. W. (1991). Paleochemistry of manganese in corals from the Galápagos Islands. *Coral Reefs*, *10*, 91–100.

Smith, L. W., Barshis, D., & Birkeland, C. (2007). Phenotypic plasticity for skeletal growth, density and calcification of *Porites lobata* in response to habitat type. *Coral Reefs*, *26*(3), 559–567. https://doi.org/10.1007/s00338-007-0216-z

Tanzil, J. T. I., Lee, J. N., Brown, B. E., Quax, R., Kaandorp, J. A., Lough, J. M., & Todd, P. A. (2016). Luminescence and density banding patterns in massive *Porites* corals around the Thai-Malay Peninsula, Southeast Asia. *Limnology and Oceanography*, *61*, 2003–2026. https://doi.org/10.1002/lno.10350

Thirumalai, K., Singh, A., & Ramesh, R. (2011). A MATLAB™ code to perform weighted linear regression with (correlated or uncorrelated) errors in bivariate data. *Journal of the Geological Society of India*, *77*(4), 377–380. https://doi.org/10.1007/s12594-011-0044-1

Thompson, D. M., Cole, J. E., Shen, G. T., Tudhope, A. W., & Meehl, G. A. (2015). Early twentieth-century warming linked to tropical Pacific wind strength. *Nature Geoscience*, *8*, 117–121. https://doi.org/10.1038/NGEO2321

Tierney, J. E., Abram, N. J., Anchukaitis, K. J., Evans, M. N., Giry, C., Kilbourne, K. H., et al. (2015). Tropical sea surface temperatures for the past four centuries reconstructed from coral archives. *Paleoceanography*, *30*, 226–252. https://doi.org/10.1002/2014PA002717

Trueman, M., & D'Ozouville, N. (2010). Characterizing the Galápagos terrestrial climate in the face of global climate change. *Galápagos Research*, *67*, 26–37.

Weber, J. N. (1973). Incorporation of stontium into reef coral skeletal carbonates. *Geochimica et Cosmochimica Acta*, *37*(1971), 2173–2190.

Wellington, G. M., Dunbar, R. B., & Merlen, G. (1996). Calibration of stable oxygen isotope signatures in Galápagos corals. *Paleoceanography*, *11*(4), 467–480. https://doi.org/10.1029/96PA01023

Wolff, M. (2010). Galápagos does not show recent warming but increased seasonality. *Galápagos Research*, *67*, 38–44.

World Meteorological Organization. (1966). Technical Note No. 79: Climatic Change, WMO No. 195.TP.100 (p. 80).

Wu, H. C., Linsley, B. K., Dassié, E. P., Schiraldi, B., & deMenocal, P. B. (2013). Oceanographic variability in the South Pacific Convergence Zone region over the last 210 years from multi-site coral Sr/Ca records. *Geochemistry, Geophysics, Geosystems*, *14*, 1435–1453. https://doi.org/10.1029/2012GC004293

Wyrtki, K. (1966). Oceanography of the eastern equatorial Pacific Ocean. *Oceanography and Marine Biology Annual Review*, *4*, 33–68.

References From the Supporting Information

Cantarero, S. I., Tanzil, J. T., & Goodkin, N. F. (2017). Simultaneous analysis of Ba and Sr to Ca ratios in scleractinian corals by inductively coupled plasma optical emissions spectrometry. *Limnology and Oceanography: Methods*, *15*(1), 116–123. https://doi.org/10.1002/lom3.10152

Chalker, B. E., & Barnes, D. J. (1990). Gamma densitometry for the measurement of skeletal density. *Coral Reefs*, *9*(1), 11–23. https://doi.org/10.1007/BF00686717

Hathorne, E. C., Gagnon, A., Felis, T., Adkins, J., Asami, R., Boer, W., et al. (2013). Interlaboratory study for coral Sr/Ca and other element/Ca ratio measurements. *Geochemistry, Geophysics, Geosystems*, *14*, 3730–3750. https://doi.org/10.1002/ggge.20230

Ku, H. H. (1966). Notes on the use of propagation of error formulas. *Journal of Research of the National Bureau of Standards. Section C: Engineering and Instrumentation*, *70C*(4), 263–273. https://doi.org/10.6028/jres.070C.025